International Journal of
MATERIALS RESEARCH

Zeitschrift für METALLKUNDE

Feature

D. A. Molodov[a], L. S. Shvindlerman[a,b]
[a] Institut für Metallkunde und Metallphysik, RWTH Aachen, 52056 Aachen, Germany
[b] Institute of Solid State Physics, Russian Academy of Science, Chernogolovka, Moscow Distr., Russia

Interface Migration in Metals (IMM): "Vingt Ans Après" (Twenty Years Later)

Dedicated to Professor Dr. Günter Gottstein on the occasion of his 65th birthday

The paper represents a comprehensive although rather brief overview of the scientific activity of the Institute of Physical Metallurgy and Metal Physics (IMM), RWTH Aachen University, in the field of grain boundary physics for the past twenty years under the leadership of Professor Günter Gottstein.

Keywords: Grain boundary; Mobility, Grain growth; Boundary energy; Triple junction

1. Introduction

This is an attempt to comprehend and describe the activity of the Institute of Physical Metallurgy and Metal Physics (IMM) of the RWTH Aachen University in the field of grain boundary physics and related phenomena in the last 20 years, when the IMM worked under the leadership of Professor Günter Gottstein. More specifically, the paper is devoted to advancement of the thermodynamics and kinetics (basically, the migration of single boundaries) of grain boundaries in metals, to 2D and 3D grain growth polycrystals, including the nanocrystals, to the evolution and stability of grain microstructure.

A criterion for the scientific directions has been to comply with several major principles:

- the experimental research should fit the reproducibility – the basic criterion of the physical experiments;
- the thermodynamic prerequisites of both the experimental and computational and simulation studies should be "transparent" and reliable;
- the phenomenological examinations are combined with the microscopic analysis of the problem;
- finally, it should be noted that preference was given to the problem which admits, at least at the original stage, a strict analytical solution.

We believe that this reasoning has made the IMM one of the main centres of the physical research in this area.

It should be noted that the current review concerns only the major, from the authors' viewpoint, fields of the scientific activity of the IMM in grain boundary physics.

The authors took an active part in the research briefly described below; they tried to be as impartial as possible in such a delicate issue. The reader will judge how much they succeeded.

2. Measurements of grain boundary motion

There are two essentially different ways to determine the position of a grain boundary in a bicrystal and to measure the grain boundary velocity. In the discontinuous method, frequently used in the past, the location of the boundary is determined at discrete time intervals by the position of a boundary groove. The advantage of this stepwise annealing method is its simplicity, but its main shortcoming is that the measured boundary velocity is averaged over the large interval of time between consecutive observations. In con-

trast, the continuous method requires determination of the boundary position at any moment in time without forcing the boundary to stop. This is achieved by utilizing orientation dependent properties and their discontinuity at the grain boundary. There are various techniques to distinguish different crystal orientations. Most measurements so far have been conducted with the XICTD (X-ray Interface Continuous Tracking Device) [1]. The method employs X-ray diffraction to determine the GB position and, therefore, does not interfere with the boundary migration process itself. The device can measure a boundary velocity in a wide range between 1 μm s^{-1} to 1000 μm s^{-1}. Its inaccuracy amounts to less than 2 % [1].

The only disadvantage of this on-line boundary tracking technique is that the boundary shape cannot be observed during its motion. For this the in-situ techniques on the basis of orientation contrast imaging can be used. In particular, the migration and shape of the grain boundaries can be measured in a scanning electron microscope (SEM) utilizing the orientation contrast revealed by an electron backscatter detector [2]. With the specially designed laser powered heating stage, in-situ investigations of grain boundary motion can be conducted at temperatures up to 1000 °C [3]. The SEM is equipped with a digital image scanning system, which records series of orientation contrast images at predetermined time intervals. In post-processing the images are analyzed by a special routine that determined the boundary velocity, from which the (reduced) boundary mobility is derived.

In materials with lower than cubic crystal symmetry, the grain boundary location can be determined from the contrast between differently oriented crystallites when illuminated by plane polarized light in an optical microscope. Recently this property has also been utilized for the polarization microscopy probe designed for use in high field magnets. It was developed to observe and continuously measure the position and shape of a magnetically driven grain boundary in a magnetically anisotropic material. The major components of the system are the polarizing microscope with a remote head video camera and the sample chamber with a resistive heater for annealing at elevated temperatures up to 500 °C in an inert gas atmosphere [4].

A driving force for grain boundary migration occurs, if the displacement of a boundary area leads to a decrease in the total free energy of the system. In most experiments which we will refer to in the following, the driving force arises either due to the curvature of the grain boundary, or from a volume free energy difference across the boundary owing to the anisotropy of free energy density in a magnetic field.

The curvature driving force for grain boundary motion is caused by the free energy of the boundary itself since boundary motion towards its center of curvature leads to a reduction in grain boundary area. Several boundary geometries were designed to move a boundary with a controlled driving force [5–7]. A constant driving force for grain boundary motion in our experiments is provided by the energy γ of a curved boundary $p_c = \gamma/a$, where a is the width of the shrinking grain (Fig. 1). The advantage of such a geometry compared to ones with a non-constant driving force [6, 7] is that the grain boundary shape remains self-similar during migration.

In the particular boundary configuration shown in Fig. 1a, the boundary with misorientation angle φ keeps its tilt character with the same angle during its motion. In the other configuration (Fig. 1b) the boundary character changes along its curved part from pure tilt to almost pure twist, although the boundary retains the same misorientation angle φ and axis <*hkl*> of rotation.

When a bicrystal of a magnetically anisotropic solid with susceptibility $\chi \ll 1$ is exposed to a uniform magnetic field, a magnetic driving force p_m arises owing to the difference of the magnetic energy density ω in adjacent grains [8]

$$p_m = \omega_1 - \omega_2 = \frac{\mu_0 H^2}{2}(\chi_1 - \chi_2)$$

$$= \frac{1}{2}\mu_0 \Delta\chi H^2 \left(\cos^2\theta_1 - \cos^2\theta_2\right) \quad (1)$$

where μ_0 is the magnetic constant, H is the magnetic field strength, χ_1 and χ_2 are the magnetic susceptibilities of adjacent grains 1 and 2 along the field direction, $\Delta\chi$ is the difference of the susceptibilities parallel $\chi_{||}$ and perpendicular $\chi_\perp$ to the principal (or c) axis of the crystal, θ_1 and θ_2 are the angles between the c-axes in both neighboring grains and the magnetic field direction. In contrast to the curvature driving force, the magnetic one does not depend on the boundary properties, i. e. on its energy and shape, but is determined by the magnetic anisotropy of the material ($\Delta\chi$), the strength of the applied magnetic field and its orientation with respect to the two grains. It moves a boundary from the grain with lower free energy toward the one with higher free energy and does not depend on the sign of the magnetic field.

Low angle symmetrical tilt boundaries are known to move under an applied mechanical stress [9–11]. They move by collective glide of the dislocations which compose these boundaries [12]. A shear stress acting on the boundary plane causes a force on each edge dislocation and thus, re-

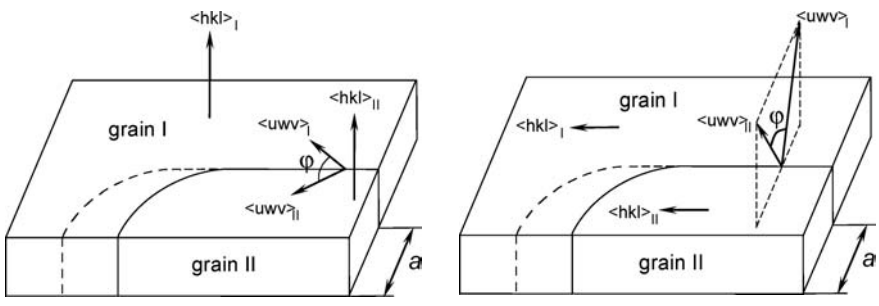

(a) (b)

Fig. 1. Bicrystal geometry with the moving curved boundary having (a) pure tilt character and (b) mixed tilt–twist character.

sults in a driving force for boundary migration [13]

$$p_s = \rho_{dis} \cdot F_{P-K} = \frac{2}{b}\sin\frac{\theta}{2} \cdot \tau b \cos\frac{\theta}{2} = \tau \sin\theta \qquad (2)$$

where ρ_{dis} is the dislocations line length per unit area in the boundary, F_{P-K} – Peach-Kohler force (per unit length) on the dislocation with a Burgers vector b [14], τ – shear stress.

3. Impact of misorientation on kinetics of <111> grain boundaries in Al

As had already been shown in the past in bicrystal experiments by Aust and Rutter [15] and by Shvindlerman with coworkers [16–18], the mobility of high angle grain boundaries depends on axis <*hkl*> and angle φ of misorientation. Studies of the mobility of tilt grain boundaries in Al bicrystals [17] have shown that the mobility of low Σ coincidence boundaries (special boundaries) exceeds the mobility of random (non-special) boundaries. Among all tilt boundaries those with <111> rotation axis and rotation angle of about 40° were found to have the highest mobility, which is associated with the special Σ7 tilt boundary.

On the other hand numerous growth selection experiments by Ibe and Lücke with coworkers [19–21] conducted on Al single crystals provided clear evidence that the maximum growth rate misorientation is close but distinctly different from the exact Σ7 orientation relationship, which occurs at an angle of rotation $\varphi = 38.2°$. The angular difference between the results is comparably small and has been attributed to the large scatter of results in growth selection experiments. Humphreys and Hatherly [22], for instance, directly connected the maximum mobility of 40°<111> tilt boundary in Al with minimum of activation enthalpy for migration of Σ7 tilt boundary. In the discussion concerning the role of 40°<111> orientation relationship in recrystallization Nes and Vatne [23] also referred to the corresponding boundary as a Σ7 special boundary. However, as already pointed out by Lücke [24], the overwhelming statistics of growth selection experiments substantiate that with progressing growth selection the fastest moving boundaries are observed for a <111> axis of rotation and for an angle $\varphi > 40°$. Although the difference between growth selection and bicrystal experiments amounts to only 2°, the difference is of prime importance with regard to the interpretation of the misorientation dependence of grain boundary mobility. The finding of a high mobility for low Σ coincidence boundaries is commonly interpreted in terms of a decreased tendency to segregation and, therefore, less solute drag in long range periodic boundary structures, as in CSL boundaries, i.e. higher boundary mobility [15]. The finding of a maximum growth rate for off-coincidence (non-special) grain boundaries would be at variance with this interpretation.

Owing to the importance of maximum growth rate boundaries for texture formation during recrystallization and grain growth this obvious discrepancy was addressed, and the misorientation dependence of grain boundary mobility on a fine scale in the angular interval 37°–43° <111> with angular spacing 0.3°–0.6° [25, 26] was investigated. The experiments revealed that the mobilities of boundaries with different misorientation angles do have different temperature dependence, and there is a temperature, the so-called compensation temperature T_c, at which the mobilities of all investigated boundaries with different misorientation are the same. As a result, at high temperature regime ($T > T_c$) the mobility is higher for grain boundaries with higher activation energy, in particular it is at maximum for $\varphi = 40.5°$, while at lower temperatures ($T < T_c$) the exact Σ7 boundary moves fastest (Fig. 2).

This result explains the apparent contradiction between growth selection experiments and recrystallization experiments. The problem resulted only from the wrong tacit assumption that the pre-exponential factor is essentially independent of misorientation so that only the activation enthalpy controls mobility. At high temperatures the grain boundary mobility in this angular interval is obviously not dominated by the segregation behavior of low Σ boundaries. The reason for the changing maximum mobility orientation in different temperature regimes is obviously the orientation dependence of both the activation enthalpy and the preexponential factor [25, 26]. The experiments re-

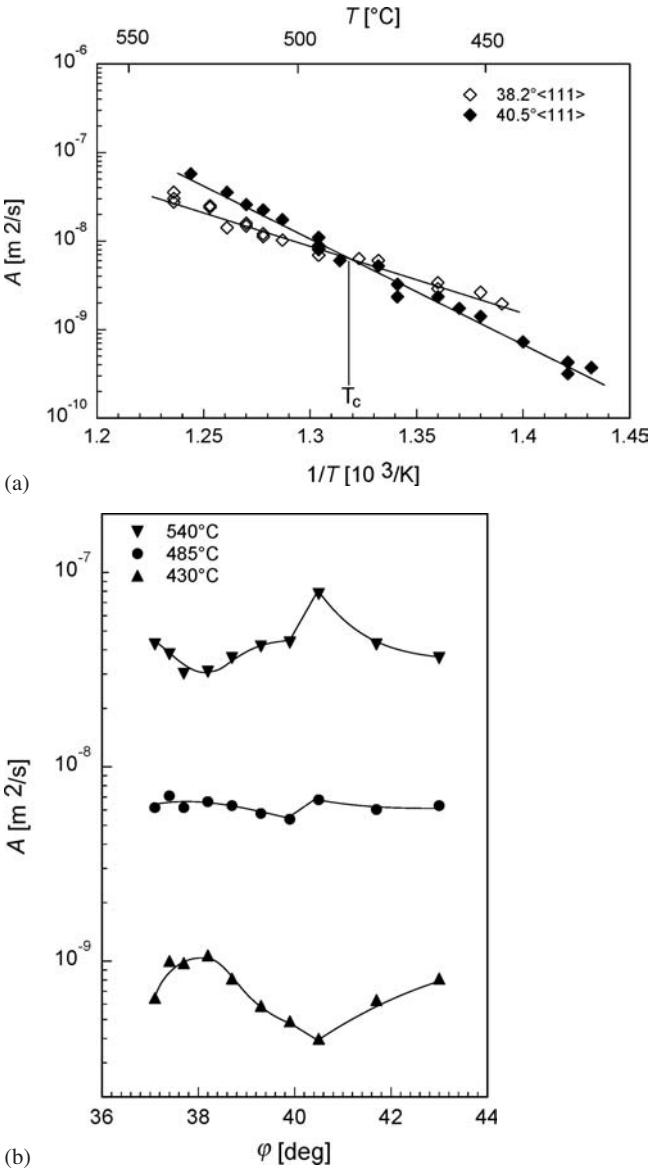

Fig. 2. (a) Temperature dependence of the reduced mobility for 38.2° and 40.5° <111> tilt grain boundaries [25] and (b) mobility dependence of <111> tilt boundaries on rotation angle in pure Al [26].

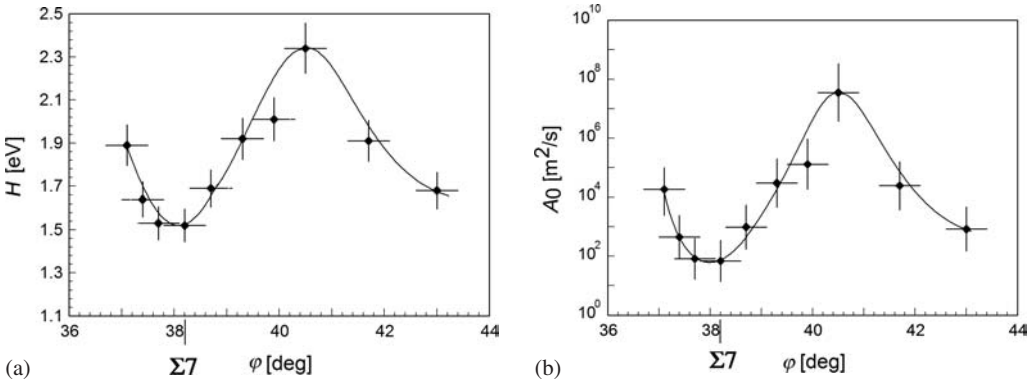

Fig. 3. (a) Activation enthalpy H and pre-exponential factor A_0 for the migration of <111> tilt grain boundaries [25].

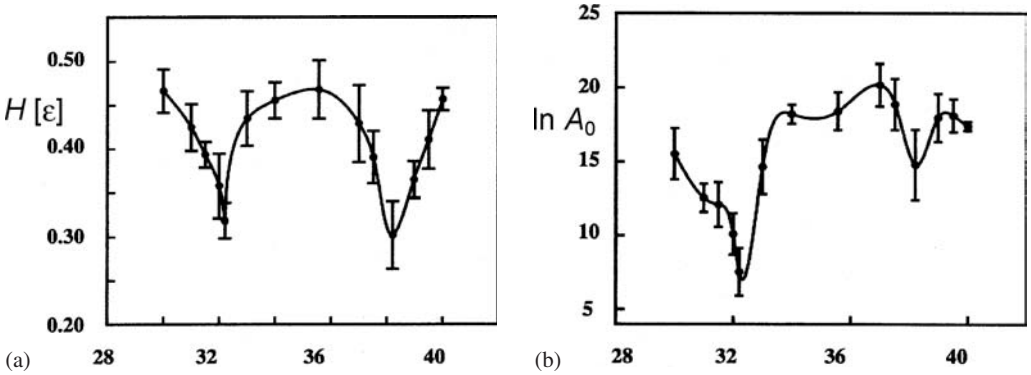

Fig. 4. (a) Activation energy of grain boundary migration ($\varepsilon = 0.57$ eV – Lennard-Jones potential well depth for Al) and (b) logarithm of the pre-exponential factor of the reduced mobility as a function of boundary misorientation found in computer simulations of grain boundary motion [28].

vealed that they were at maximum for a misorientation angle $\varphi = 40.5^\circ$ and at minimum for the exact Σ7 misorientation (Fig. 3). Growth selection experiments by Ibe et al. [19–21] were conducted at very high temperatures (above 600 °C), i. e. in the temperature regime where the mobility of the 40.5° <111> boundary is in fact the highest due to its highest (activation enthalpy and) pre-exponential factor (Figs. 2 and 3) [25, 26].

The misorientation dependence of grain boundary motion is not confined to pure tilt boundaries. The experiments on Al-bicrystals with a grain boundary configuration shown in Fig. 1b revealed that the motion of <111> boundaries in Al in the vicinity of Σ7 misorientation depends non-monotonically on misorientation angle irrespective of the crystallographic configuration of the curved moving boundary, whether pure tilt or mixed tilt–twist [27]. Both activation parameters for the motion of <111> mixed tilt–twist boundaries were observed to change non-monotonically with misorientation angle and assume a minimum at the Σ7 misorientation [27] that is very similar to the respective misorientation dependence for <111> tilt boundaries in Fig. 3. Therefore, the curved boundaries in both configurations (Fig. 1), pure tilt with differently inclined boundary elements and mixed tilt–twist, demonstrate essentially the same behavior with regard to the misorientation dependence of their motion.

The non-monotonic dependence of grain boundary motion on misorientation angle was also confirmed by computer simulations of curvature driven boundary migration [28]. As depicted in Fig. 4, the activation energy and the logarithm of the pre-exponential factor of boundary mobility exhibited very similar variations with misorientation, including the presence of distinct cusps at low Σ misorientations.

4. Compensation effect in grain boundary migration

The temperature dependence of grain boundary mobility m follows an Arrhenius relation

$$m = v/p = m_0 \exp\left(-\frac{H}{kT}\right) \tag{3}$$

where v is the boundary velocity, p is the driving force, H is the activation enthalpy of grain boundary migration and m_0 the corresponding pre-exponential mobility factor[1].

Since the exact magnitude of the boundary energy is usually not known, in experiments with curved boundaries (Fig. 1) the reduced boundary mobility is determined

$$A \equiv v \cdot a = m \cdot \gamma = A_0 \exp\left(-\frac{H}{kT}\right) \tag{4}$$

Commonly, for evaluation of experimental data the activation enthalpy H is determined from the slope of the Arrhenius plot, and much less attention is paid to the pre-exponential factor m_0 (A_0). However, there is a large body of experimental evidence that the pre-exponential factor is strongly related to the activation enthalpy: it increases or decreases, if the activation enthalpy increases or decreases according to relation

$$H = \alpha \ln A_0 + \beta \tag{5}$$

where a and β are constants.

[1] It is worth noting that the activation enthalpy depends on pressure P, $H = E + PV^*$, where E is the activation energy and V^* the activation volume for grain boundary motion. Therefore, measurements of the pressure dependence of grain boundary velocity at a given temperature provide the opportunity to derive the activation volume V^* [16, 29].

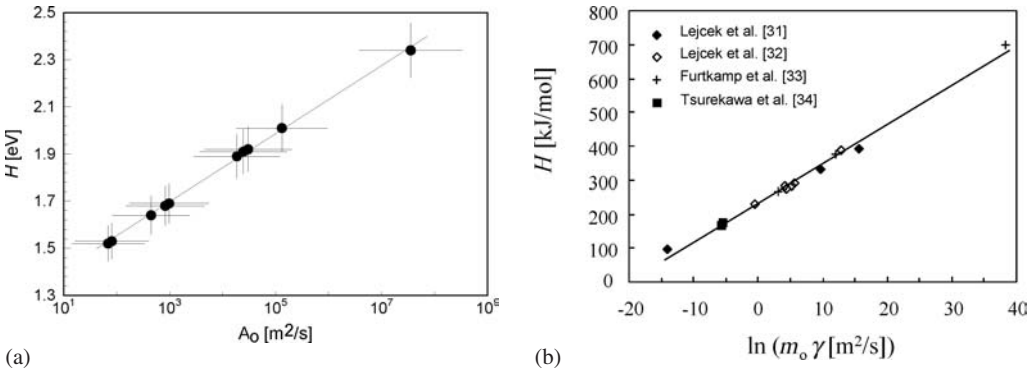

Fig. 5. Compensation relationship between the activation enthalpy and the pre-exponential factor for the motion of (a) <111> tilt grain boundaries in Al [26] and (b) <001> tilt grain boundaries in Fe-3.5 % Si [31–34].

This correlation is referred to as the compensation effect, since it strongly moderates the effect of a variation of H on the value of the mobility, and therefore allows one to use annealing temperature as a selective tool for grain boundary control.

The compensation effect was repeatedly observed in various thermally activated processes, but it is most strongly pronounced in processes related to interfaces and grain boundaries. Fig. 5a depicts the compensation effect for <111> tilt boundary migration in the vicinity of the special misorientation Σ7. It was found that the compensation rule holds also for Bi [30], Sn [16] and Fe-3.5 % Si (Fig. 5b) [31–34]. Also, the compensation effect was observed in molecular dynamics simulations of curved boundary motion [35]. It is worthy of note that the compensation effect was also observed for the change of the activation parameters of ^{71}Ge diffusion along <111> tilt grain boundaries with different angles in the vicinity of the Σ7 misorientation in pure Al (Fig. 6) [36]. The experimental data presented above can be comprehended on the basis of approach put forward in Ref. [37].

A consequence of the specific linear dependence between the activation enthalpy and the logarithm of the pre-exponential factor is the existence of the so-called compensation temperature $T_c = \alpha/k$, at which the mobilities are equal and at which the kinetic lines in Arrhenius co-ordinates intersect at one point (Fig. 2).

The observed coupling of entropy and enthalpy of activation suggests that the activated state is not a random energy fluctuation in space and time, but a definite and thus reproducible although unstable state, which is described by its respective thermodynamic functions. Its attainment from the stable ground state can be associated with a first order phase transformation. In an interface we can associate the activated state with a local change of the interface structure, or more precisely, of a structure that the interface could attain if not a more stable state would exist for the given thermodynamic conditions. In this concept the compensation temperature is the equilibrium temperature for such a virtual phase transformation. The linear compensation relation and the expression for the compensation temperature can be derived under these conditions [37]. In particular, the compensation temperature can be expressed as $T_c = \mathrm{d}H/\mathrm{d}S|_{\lambda=\lambda_0}$, where the parameter λ denotes some intensive structural or chemical specification, such as angle of misorientation, composition, etc. The derived equations [37] manifest a linear relation between the enthalpy and entropy of activation. It was shown that in analogy to the temperature compensation effect for constant pressure there is also a pressure compensation effect for constant temperature at variable pressure. In fact, such a relation was experimentally verified [38]. It is of interest that the major relation of the theoretical approach can be derived, using the Onsager principles for non-equilibrium thermodynamics, i.e., the principle of maximum rate of change the thermodynamic potential of the system. It was shown that the Mott "island" model complies with the compensation effect [38]. The model assumes that groups of n atoms "melt" on the side of the vanishing grain and become attached to the side of the growing one. The activated, metastable state is identified with a frozen liquid state. This permits determination of the entropy and energy of activation, namely

$$S^* = \frac{nL}{T_m}, \quad H^* = nL \tag{6}$$

where L is the heat of melting per atom and Tm the melting temperature. It is clear that Mott's model complies with the compensation effect: the enthalpy of activation is proportional to the activation entropy and the compensation temperature coincides with melting temperature:

$$H^* = T_m S^* \tag{7}$$

$$T_c = \frac{\mathrm{d}H^*}{\mathrm{d}S^*} = T_m \tag{8}$$

The well-known empirical relations of Brown and Ashby for diffusion data (for a given structure and bond type) are valid for a wide range of solids:

$$\begin{aligned} D(T_m) &= k_1 \\ \frac{H^*}{kT_m^0} &= k_2 \\ V^* &= \frac{H^*}{T_m^0}\left(\frac{\mathrm{d}T_m^0}{\mathrm{d}p}\right) \end{aligned} \tag{9}$$

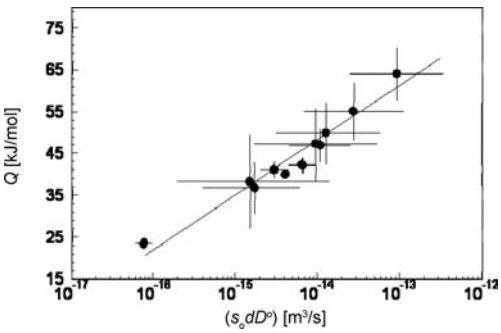

Fig. 6. Relationship between the activation enthalpy and the pre-exponential factor of 71Ge diffusion along tilt grain boundaries in the vicinity of the Σ7 CSL-orientation in pure Al [36].

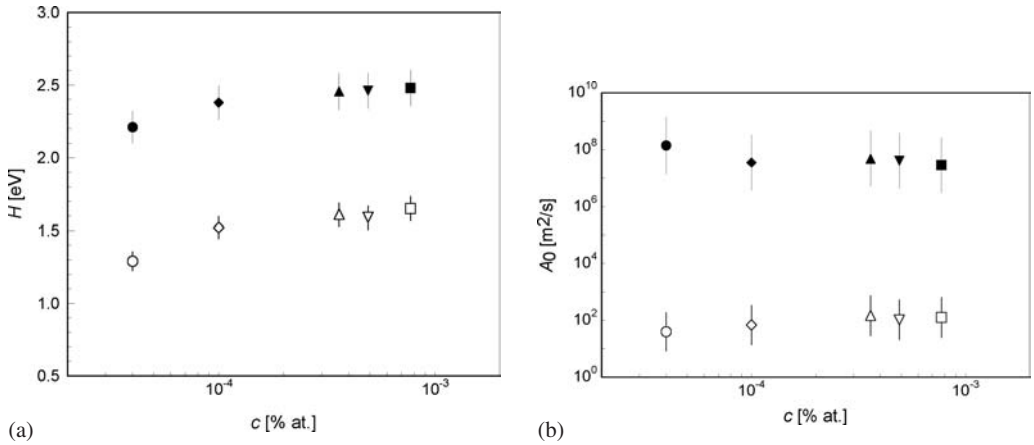

(a) (b)

Fig. 7. The dependence of (a) activation enthalpy and (b) mobility pre-exponential factor for migration of 38.2° (open symbols) and 40.5° (filled symbols) <111> tilt grain boundaries on impurity concentration in differently pure aluminium [26].

where k_1 and k_2, are constants, T_m^0 is the melting point at atmospheric pressure.

As has been shown [37], these relations are in the full agreement with the concept of the compensation effect and can be considered as a direct consequence of this effect.

However, the major success is the explanation on the basis of the compensation effect the contradiction between the bicrystal measurements of the activation enthalpy and grain boundary mobility measured in polycrystal experiments (see Section 3). It is worthy of note that compensation effect transforms the traditional notions of how the activation energy (enthalpy) affects the kinetics of the processes. The compensation temperature T_c divides the temperature range into two intervals. If the experiments are conducted below the T_c, then the processes with low enthalpy of activation are the fastest; if the measurements are taken above T_c, then the processes with high activation enthalpy dominate. There is a large body of experimental evidence that the compensation temperature is often close to the equilibrium temperature of a nearby phase transition. In particular, for Sn and Bi the compensation temperature is practically equal to the respective melting temperature [16, 30].

5. Impurity effects on orientation dependence of boundary mobility

The common understanding of the orientation dependence of grain boundary mobility and the effect of solutes on this dependence is mainly founded on the classical work of Aust and Rutter [39, 40] as well as on results of experiments by Fridman et al. [41]. According to this understanding the orientation dependence of grain boundary mobility is a segregation effect: strongly ordered boundaries, i. e. low Σ coincidence boundaries segregate less and, therefore, move faster than random boundaries.

This classical concept, however, cannot be confirmed by results of experiments [26] and computer simulations [28]. The experimental results reveal that the migration activation enthalpy is strongly affected by both the boundary crystallography and material purity. However, with changing misorientation angle the pre-exponential factor A_0 rises with increasing H by several orders of magnitude (Fig. 3), while with changing impurity content A_0 remains at the same level (Fig. 7) [26]. Therefore, the pre-exponential factor A_0 in the investigated impurity concentration interval was found to be much less sensitive to the material purity than to a change in the misorientation angle. This result allows the conclusion that the observed orientation dependence of mobility (Figs. 2 and 3), determined by both H and A_0, does not simply reflect the different segregation behavior of coincidence and random boundaries, as frequently proposed [39, 40], rather it provides evidence for an intrinsic dependence of grain boundary mobility on grain boundary structure. Also, molecular dynamics simulations of boundary motion in absolutely pure material reveal strong evidence for the intrinsic structural character of the orientation dependence of boundary mobility [28].

Aust and Rutter attributed the abnormally high values of activation enthalpy for grain boundary motion in lead to impurity effects on this process and interpreted their results in terms of diffusional mechanisms of boundary motion [40]. However, such interpretation requires attributing the difference of activation enthalpy measured for different boundaries to the adsorption energy of impurity atoms in the pure boundary. This energy normally does not exceed 0.4–0.6 eV [42]. The difference in the activation enthalpy of motion for different boundaries in the experiment of Aust and Rutter amounts to 42.8 – 5.2 = 37.6 kcal/g-atom (1.63 eV) and thus, is too large to be interpreted as adsorption energy of impurities.

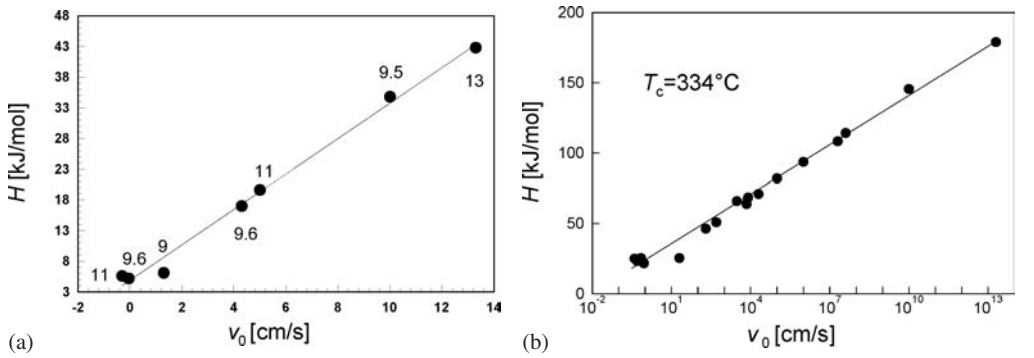

(a) (b)

Fig. 8. Relationship between the migration activation enthalpy H and preexponential factor v_0 of the velocity equation for migration of grain boundaries in Pb as obtained from an analysis of results of Aust and Rutter [40] (a) for different boundaries in Pb of equal purity (concentration of Sn in Pb in ppm is noted in the Figure), and (b) for all 17 measured boundaries in Pb with different crystallography and concentration of Sn from 1 to 13 ppm.

On the other hand, all 17 boundaries investigated in Ref. [40] were crystallographically different and the compensation effect, which obviously reflects the thermodynamic fundamentals of the migration mechanisms for boundaries with different grain misorientation, holds for the migration parameters in the work of Aust and Rutter as well (Fig. 8). The compensation effect for migration of crystallographically different boundaries in lead of almost equal purity (9–13 ppm) in Aust and Rutter's experiment (Fig. 8a) provides unambiguous evidence that the activation parameters do not increase due to an increase in tin concentration in lead, rather than due to different boundary crystallography. Actually, the compensation effect is observed for migration parameters of all 17 boundaries investigated by Aust and Rutter, irrespective of tin concentration, with a compensation temperature $T_c = 334\,^{\circ}\mathrm{C}$ which by practical means is identical with the melting point of Pb (327 °C) (Fig. 8b).

6. Effect of boundary orientation on curved boundary motion

Grain boundary mobility is known not only to depend on misorientation, but also on the inclination of the grain boundary plane [43]. In experiments with curvature driven boundaries the moving curved part of the boundary consists of different boundary planes, the average mobility over all differently inclined boundary planes is measured and it is assumed that there is uniform tilt grain boundary mobility. This can be proved experimentally if the orientation of the entire moving curved boundary will be changed by an inclination of the initial flat tilt boundary from its symmetrical position ($\psi > 0$, Fig. 9). Therefore, the motion of different sets of boundary planes for the same φ <*hkl*> tilt boundary can be measured and compared. Moreover, it is easily seen that even in the case of symmetrical flat boundary for all rotation axes other than <100> the sets of boundary planes comprised in the curved boundaries moving in the opposite directions (Fig. 9) are different. The larger ψ, the more difference in the orientation of correspondent curved sections. If the boundary mobility depends on boundary inclination, this can affect the velocity of steady state motion of a curved boundary.

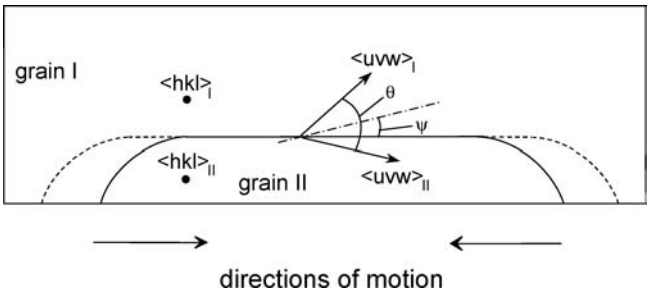

Fig. 9. Motion of curved tilt boundary with different sets of boundary planes. The straight section of the boundary is asymmetrical with an inclination ψ from symmetrical position.

The results of measurements of the motion of some high angle <111> tilt boundaries in opposite directions [27] revealed practically no difference in the migration of curved boundary, neither in the case of symmetrical initial straight boundary nor in the case of asymmetrical boundaries with inclination angle up to $\psi = 7.1^{\circ}$ [27]. Similar behavior was observed for the motion of 46.5° <111> tilt boundary in Al in the same geometry with the straight boundary having different inclination angles [44]. Therefore, on Al bicrystals it has been experimentally confirmed that the change of the set of boundary planes in the curved moving boundary does not affect its motion.

Since twist boundaries are by definition planar, it is impossible to directly measure their motion by utilizing grain boundary curvature as a driving force. However, a change of a bicrystal geometry provides the opportunity to study the motion of mixed boundaries comprising both tilt and twist components (Fig. 1b). In such a configuration the boundary character changes along its curved part from pure tilt to almost pure twist. As mentioned in Section 3, the motion of <111> boundaries in configuration Fig. 1b has been studied in the angular interval of misorientation between 37 and 42° [27]. In particular the shape of the curved moving part of the boundary was measured and compared with the boundary shape which was calculated analytically [45]. The shape of a boundary $y(x)$ (Fig. 10) can be derived from the equation of motion

$$y'' = -\frac{v}{m\gamma} y'(1 + (y')^2) \qquad (10)$$

under the relevant boundary conditions [45], assuming that the grain boundary energy γ and mobility m are independent of the orientation of the grain boundary relative to the crystallographic axes of the grains. The consistency of measured and calculated boundary shape leads to the conclusion that different elements of the investigated curved boundary have the same mobility, irrespective of their composition of tilt and twist components. That means, an increase in the twist component along the curved mixed boundary in such geometrical configuration does not affect its steady-state motion.

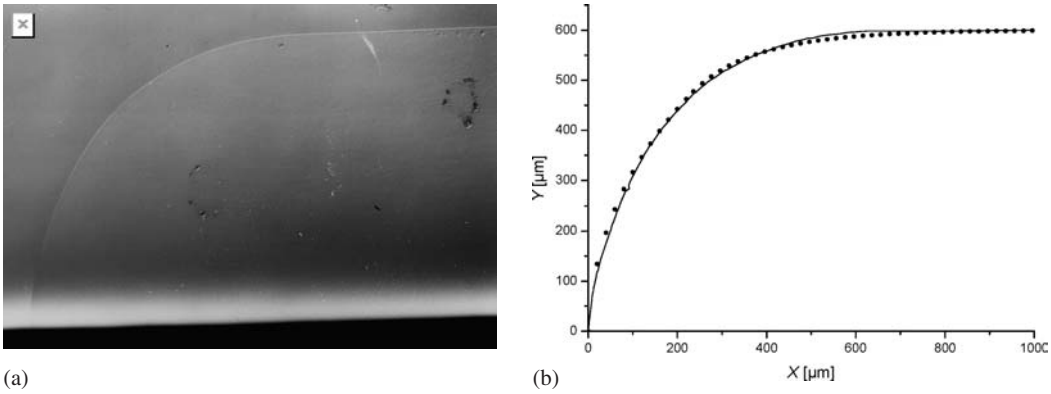

(a) (b)

Fig. 10. (a) Measured and (b) calculated shape of a moving 40.6° <111> mixed tilt–twist boundary in pure Al (99.999 %) at $T = 602\,^{\circ}\mathrm{C}$ [27].

7. Shape and kinetics of <100> and <111> tilt boundaries with misorientations in the transition range from low to high angles

Recent experimental in-situ observations on <100> and <111> tilt grain boundaries with misorientation angles in the range between 6° and 24° revealed that from all investigated boundaries only those with misorientation angle $\theta > 15°$ can assume a curved configuration (Fig. 1) and steadily move under the curvature driving force [46, 47]. In the entire investigated temperature range these boundaries moved steadily and their smoothly curved shape remained self-similar during the motion.

Two boundaries with smaller angles, 14.3° <100> and 13.8° <111>, were observed to assume a curved shape and to move under the curvature driving force only at temperatures above 600 °C and 590 °C, respectively. All other investigated boundaries with smaller misorientation angles do not assume a curved configuration in the entire temperature range up to the melting point and, thus, do not move under a capillary driving force. These low angle boundaries retained their initial flat configuration or, with rising misorientation angle, formed additional facets inclined to the initial boundary orientation (Fig. 11).

Computational analysis provided evidence that the experimentally observed shape of low angle boundaries and its evolution with increasing misorientation can be attributed to the inclination dependence of grain boundary energy. The simulations revealed a distinct energy anisotropy of <100> and <111> low angle boundaries with respect to their inclination [47]. The degree of anisotropy changes with misorientation angle and becomes maximum for low angle boundaries where the energy attains a distinct minimum for specific symmetrical configurations, i.e. $\psi = 45°$ for <100> and $\psi = 0°$ for <111> boundaries. Therefore, the boundaries with small misorientation remain straight at any temperature up to the melting point, since their energy in the initial symmetrical configuration is minimal. With rising misorientation angle the inclination dependence of the boundary energy decreases, and when the energy of <100> tilt boundaries in both symmetrical configurations becomes comparable the boundary forms an almost planar segment with inclination close to $\psi = 0°$ (Fig. 11a). Analogously, in the case of <111> tilt boundaries, a weaker dependence $\gamma(\psi)$ with misorientation angle leads to the formation of a planar segment with ψ close to 60° (Fig. 11b).

The faceted <100> and <111> tilt boundaries were observed not to move at constant temperature [46, 47], although also a faceted grain boundary system is subject to a driving force, since the displacement of the facet is associated with an overall decrease in the free energy. Apparently, an individual boundary element on a facet does not experience a local driving force, since its displacement would increase the grain boundary area. The motion of a flat facet under the capillary driving force, therefore, requires a mechanism different from the motion of curved grain boundaries. Steps have to be introduced on the facet, the lateral motion of which will displace the facet. While the motion of steps proceeds generally very quickly, the generation of these steps may have an impact on the displacement rate of the facet. If steps can be easily generated, e.g. when the facet borders a curved boundary, the facet velocity may actually be high [48, 49]. In the case of sharp vertices, however, step generation can be difficult and thus, the facet mobility will be low.

A further increase in misorientation is accompanied by a reduction in the energy anisotropy, and boundaries with misorientation $\theta > 15°$ can convert to the curved configuration and move steadily at constant temperature under the curvature driving force [46, 47].

The investigated behavior and migration parameters of <100> and <111> tilt boundaries with misorientation angles in the range between 6° and 24° can be compared with literature data. Fridman et al. [41] have measured the mobility of curvature driven <100> tilt boundaries in bicrystals of high purity Al using a discontinuous method, i.e. the boundary location was determined in discrete time intervals from the position of the boundary groove on the surface of the bicrystals. The measured boundary velocity in this step-wise annealing method was averaged over the time between consecutive observations. The same method was used by Aristov et al. [17] for measurements of the migration of <111> tilt boundaries in Al bicrystls. The <111> tilt boundaries in Al were also investigated by Winning et al. [50], who utilized X-ray diffraction for tracking a moving grain boundary [1].

As seen in Fig. 12, the results of in-situ SEM measurements of the motion of high angle ($\theta > 16°$) <111> tilt boundaries are in a good accordance with results of experiments by Aristov et al. [17] and Winning et al. [50]. In contrast, the activation enthalpy for the motion of <100> tilt boundaries in a similarly pure Al in our study was found to be much higher than that in experiment by Fridman et al.

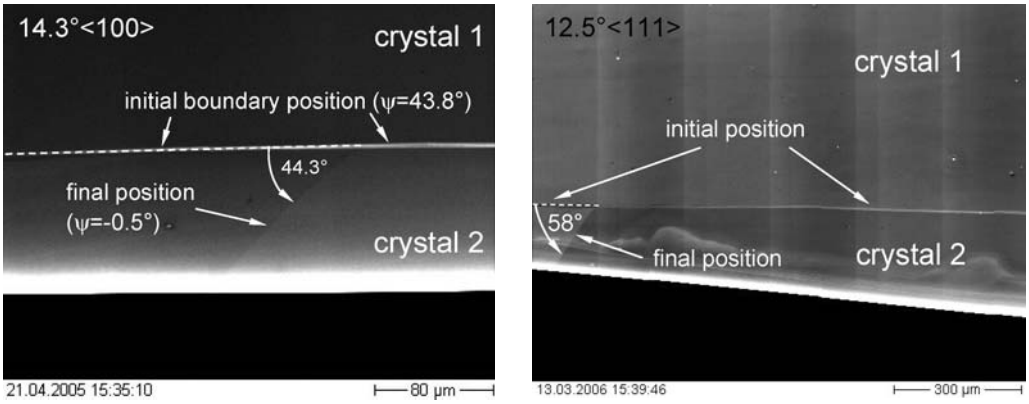

Fig. 11. Single facet configuration of (a) 14.3° <100> tilt boundary at 450 °C and (b) 12.5° <111> tilt boundary at 520 °C [47].

[41]. (Moreover, the values of the migration activation enthalpy obtained by Fridman et al. for <100> tilt boundaries with θ between 33° and 44° (0.7 – 1.4 eV) [41] also cannot be confirmed by the recent in-situ measurement [51], which revealed for the migration activation enthalpy values in the range between 2.0 and 2.7 eV).

However, the major disagreement between results of the experiment by Kirch et al. [46, 47] and previous investigations by Fridman and Winning is that they both reported about the steady-state motion of small angle ($\theta < 14°$) tilt boundaries under the constant curvature driving force. The reported behavior of <100> and <111> boundaries is, however, essentially different. While 10° and 12° <100> boundaries in the experiment by Fridman moved slower with higher activation parameters (activation enthalpy and pre-exponential mobility factor) than the boundaries with $\theta \geq 15°$ (Fig. 12a), for 6° and 12° <111> boundaries in the study by Winning were obtained much lower activation parameters than for large angle boundaries (Fig. 12b), so that a 6° <100> boundary moved substantially faster than a 14° <100> boundary, whose migration activation enthalpy was attributed to the high angle branch of the $H(\theta)$ – dependence [50].

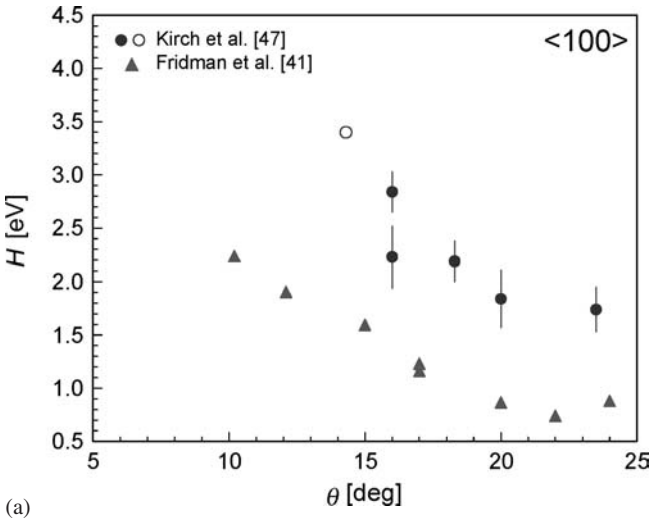

(a)

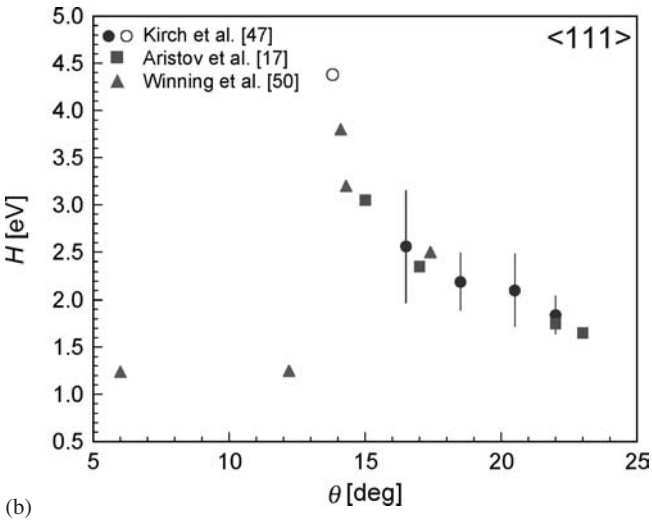

(b)

Fig. 12. Migration activation enthalpy H for investigated <100> and <111> tilt grain boundaries. For 14.3°<100> and 13.8°<111> boundaries (non-filled circle symbols) the activation enthalpy was determined from mobility values measured at two temperatures, 600 °C and 610 °C, and 600 °C and 620 °C, respectively.

Unfortunately, there is an extreme lack of further experimental data to be compared with the recent observations and measurements [46, 47]. This is obviously due to specific difficulties of a bicrystal experiment and a lack of the appropriate measuring methods. It must, however, be stressed that in the study by Kirch the utilizing of the most advanced SEM technique for true in-situ observations at elevated temperatures revealed unambiguously that among <100> and <111> tilt boundaries with misorientations in the range between 6° and 24° only high angle ($\theta > 15°$) boundaries can assume the curved shape and steadily move under the capillary driving force.

Classical theories of grain growth assume that grain boundary energies are isotropic. However, as a result of recent experiments and computer simulations it has been recognized that the anisotropy of boundary properties can be essential for grain growth in polycrystals and determine the final distribution of boundaries with respect to their character [49, 52, 53]. A faceting behavior was repeatedly reported for grain boundaries with misorientations close to low S CSL orientation relationships [54]. However, the experiments and computer simulations [46, 47] demonstrated that the inclinational anisotropy of grain boundary energy also applies to low angle tilt boundaries with low index rotation axis. The restricted ability of low angle boundaries to move has to be accounted for in an analysis or modeling exercise of microstructural evolution during grain growth, especially in highly textured polycrystals.

8. Effect of faceting on curvature driven boundary motion in Zn

The facets reflect the crystalline nature and reflect an anisotropy of the surface energy, they have been observed on internal surfaces, in particular on grain boundaries and manifest themselves as straight grain boundary segments [55]. The relation between grain boundary faceting and grain boundary behavior, in particular, grain growth and grain boundary migration has been the subject of investigation in the past [49, 52, 56 – 60]. It was demonstrated, in particular, that the rather complicated kinetics of grain boundary motion, in particular the strong non-Arrhenius temperature dependence, could be explained by considering the motion of two competitive facets [49]. Rabkin considered the influence of grain boundary faceting on grain growth and the motion of a 2D grain boundary half-loop [49].

The distinctive property of the study [48, 61] is the steady-state motion of the individual grain boundary – grain boundary half-loop.

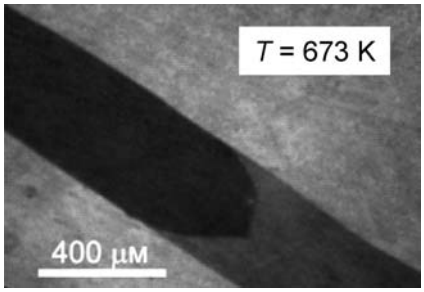

Fig. 13. Video frame of a moving grain boundary half-loop with facets [61].

One of the main advantages of such a configuration is a possibility to obtain a strict analytical solution for all parameters of a moving grain boundary and, as a result, to construct a clear physical picture of the phenomenon. The steady state motion of the $[10\bar{1}0]$ and $[11\bar{2}0]$ tilt grain boundary half-loop in Zn bicrystals was recorded in-situ (Fig. 13).

The physical model of the faceted boundary used in [48, 61] admits a strict analytical solution for the shape of the moving grain boundary and its parameters. Combining this solution with the so-called weighted mean curvature approach we can express the velocity of the facet and its length as (Fig. 14):

$$V = \frac{m_f \gamma \sin\varphi \sin\theta}{l}, \quad l = \frac{\frac{a}{2}}{\sin\theta + \frac{m_b(\theta-\varphi)}{m_f \sin\varphi \sin\theta}} \tag{11}$$

Equation (11) opens the door to deriving the mobility of the facet and its temperature dependence from the experimentally measured values of the facet length. For example, the normalized facet mobility (m_f/m) for the facet in grain boundary system $[10\bar{1}0]$ extracted from the experimental data is presented in Fig. 15 [48].

The absolute value of the facet mobility can be extracted if the grain boundary mobility is known from an independent experiment [48]. The results show that the motion of the facets is activationless, that suggests that the migration of the facet, i. e. displacement rate normal to itself, proceeds through step motion along the facet. The major conclusion inferred from these experiments: the decrease in the facet length is only due to an increase in the mobility of the curved boundary. In Ref. [61] it was shown that the dynamic facet length given by Eq. (11) is equivalent to a maximum rate of free energy decrease.

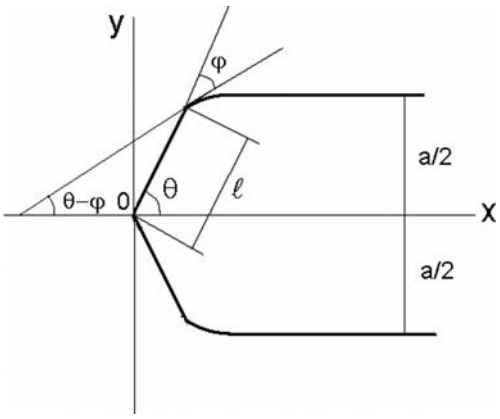

Fig. 14. Geometry of a grain boundary half-loop with a facet [48].

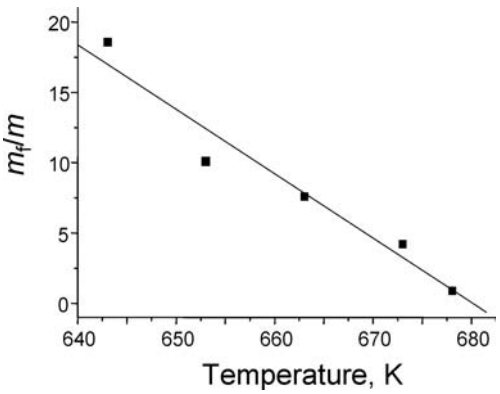

Fig. 15. Temperature dependence of the ratio of the facet normalized mobility m_f/m for the 30° $[10\bar{1}0]$ tilt grain boundary [48].

As shown in [38] the velocity of the half-loop as a whole V complies with the extremum of the function

$$(V) = \left[2\gamma_b V - a\int_0^V \frac{V\,\mathrm{d}V}{M(V)}\right] \tag{12}$$

Only maxima of this function correspond to stable steady-state motion. For a linear dependence of the velocity on the driving force ($M(V)$ = const.) the extremum of the function $\Psi(V)$ is equivalent to the **maximum rate of reduction of free energy of the system (dissipation rate)**, which in turn is related to the Onsager principle of irreversible thermodynamics. In other words, the system tries to reduce the free energy as fast as possible, i. e. with the maximum possible rate. For the steady-state motion of a grain boundary half-loop with a facet the average mobility of $M(V)$ can be defined in two ways, either by the facet motion or by the motion of the curved boundary. A maximum rate of free energy reduction of the system is obtained for a constant average mobility:

$$M_f(V) = M_b(V) \tag{13}$$

Obviously condition (13) is satisfied by relation (11). In essence, the facet changes its length in the course of motion in order to permit the system to reduce its free energy with the highest rate.

9. Magnetically driven grain boundary motion in Bi and Zn bicrystals

Since the magnetic driving force is induced by an external field and does not depend on boundary properties, the method provides an opportunity to investigate the motion of specific planar grain boundaries with well-defined structures and to determine their absolute mobility. The motion of such boundaries was first measured by applying a strong magnetic field to specially prepared bismuth bicrystals [30, 62]. Since bismuth is known to possess the largest magnetic anisotropy with different susceptibilities parallel and perpendicular to the trigonal axis (at 252 °C $\Delta\chi = 0.23 \times 10^{-4}$) [63], it is a most suitable material for a model experiment to measure a magnetically driven grain boundary migration. Symmetrical and asymmetrical pure tilt boundaries with a 90° <112> misorientation were examined.

The experiments unambiguously confirmed that the grain boundaries in the investigated bicrystals actually moved under the action of a magnetic driving force (Fig. 16a). The observed linear dependence of the boundary displacement with annealing time proves the free character of its motion. The possibility to change the magnitude of the driving force for boundary migration by exposing the samples to magnetic fields of different strength yields the unique opportunity to change the driving force on a specific grain boundary and, thus, to obtain the driving force dependence of grain boundary velocity $v = v(p)$. The measurements of boundary migration in different magnetic fields

confirmed that the boundary velocity changes linearly with the driving force. Therefore, from these results the absolute value of the grain boundary mobility $m = v/p$ can be immediately extracted, and the dependence of grain boundary mobility on temperature and on the specific grain boundary character can be determined.

The temperature dependence of the mobility of a symmetrical and an asymmetrical 90° <112> tilt grain boundary revealed that the migration parameters (activation enthalpy H and mobility pre-exponential factor mo) for the symmetrical boundary ($H = 0.51$ eV, $m_o = 0.67\ m^4\ J^{-1}\ s^{-1}$) drastically differed from the migration parameters for the asymmetrical boundary ($H_{\parallel} = 3.38$ eV, $m_{o\parallel} = 2.04 \times 10^{24}\ m^4\ J^{-1}\ s^{-1}$ and $H_{\perp} = 3.79$ eV, $m_{o\perp} = 1.10 \times 10^{28}\ m^4\ J^{-1}\ s^{-1}$, where the symbols $\parallel$ and $\perp$ refer to the orientation of the c-axis with regard to the boundary plane normal, as referred to below). As a consequence, the symmetrical boundary has a much higher mobility than the asymmetrical boundary in the entire investigated temperature range up to the melting point of bismuth but particularly at low temperatures (Fig. 16b). Clearly, the inclination of the tilt boundary in Bi has a very strong influence on its mobility [30].

The most surprising feature is that in contrast to the symmetrical boundary, for an asymmetrical tilt boundary the measured mobility was found to be distinctly different for the motion in opposite directions [62]. For the chosen crystallography of the bicrystals the boundary was less mobile when the c (<111>) axis in the growing grain was perpendicular to the direction of motion ($m_{\perp} = 8.2 \times 10^{-9}\ m^4\ J^{-1}\ s^{-1}$ at 252 °C) but faster, when the trigonal c-axis in the growing grain was close to the direction of motion ($m_{\parallel} = 1.3 \times 10^{-8}\ m^4\ J^{-1}\ s^{-1}$ at 252 °C). There are several potential reasons for this anisotropy. First, there is an essential difference in the distance between the crystallographic planes on each side of the boundary. Estimation shows that this factor may change the velocity of grain boundary motion, however this difference is unlikely to affect the velocity of boundary motion by more than 20 %, which is distinctly less than the observed effect. Second, because boundary motion in Bi-bicrystals may be influenced by impurity drag, the difference in the diffusivity of impurities in two opposite directions in the anisotropic structure of Bi should be taken into account. Finally, as shown in Ref. [64], the motion of a grain boundary in a magnetic field can be considered as a motion of a conductor in a magnetic field, or more strictly, as the motion of a region with a conductivity different from that of the surrounding matrix in a magnetic field. Such a motion causes an electromotive force and as a consequence, an additional dissipation of energy in a magnetic field [64]. This dissipation means a decrease in the effective driving force for grain boundary motion. With respect to the proportionality between grain boundary migration rate and the applied driving force this appears like decreased grain boundary mobility. This effect, however, depends on the orientation of the magnetic field with regard to the crystal axes and, therefore, on the direction of motion. Consequently, this causes a different apparent mobility for boundary motion in opposite directions. The energy dissipation should, on the one hand, be different for symmetric and asymmetric boundaries and, on the other hand, be different for boundary motion in opposite directions for asymmetric boundaries [64]. The predicted effect, however, is much smaller than experimentally observed. Therefore the observed mobility asymmetry for asymmetric tilt boundaries in Bi has to be attributed to other reasons. In any event, if this asymmetry of grain boundary mobility holds also for other metals, it will have a serious impact on our understanding of grain boundary motion, since the mobility of a grain boundary is commonly conceived as not dependent on its direction of motion.

In further bicrystal experiments it has also been shown that in zinc the magnetic anisotropy is pronounced well enough to drive boundaries in the presence of magnetic fields of attainable strengths. Hexagonal, diamagnetic zinc has a different magnetic susceptibility parallel and perpendicular to its c-axis such that $|\chi_{||}| > |\chi_{\perp}|$. Susceptibility measurements of high purity zinc crystals have shown that the volume susceptibility difference of about $\Delta\chi = 0.5 \times 10^{-5}$ remained virtually constant up to $0.95T_m$ [65].

The mobility of a magnetically driven symmetrical near coincidence Σ15 (86°<11$\bar{2}$0>) tilt grain boundary has been measured to be very low, while asymmetrical 89° <10$\bar{1}$0> tilt boundaries were observed to be quite mobile [66, 67]. The mobility of 89° <10$\bar{1}$0> tilt boundary was determined to be about $m = 2.5 \cdot 10^{-8}\ m^4\ J^{-1}\ s^{-1}$ [67]. For comparison, the reduced mobility $A_b = m \cdot \gamma$ of a curved 86° <10$\bar{1}$0> tilt boundary at 400 °C in a Zn bicrystal was measured to be $A_{bZn}^{400C} = 3.2 \cdot 10^{-8}\ m^2\ s^{-1}$ [68]. Assuming boundary energy of $\gamma \cong 0.46\ J\ m^{-2}$ [69] this yields an absolute mobility of $m_{Zn}^{400C} \cong 7.0 \cdot 10^{-8}\ m^4\ J^{-1}\ s^{-1}$, which is in reasonable agreement with the value measured for the plane boundary.

It is worth noting that the mobility of 89° <10$\bar{1}$0> tilt grain boundaries with the same misorientation but different boundary orientations was found to be distinctly different depending on the degree of boundary asymmetry, namely, the boundary with larger inclination with respect to symmetrical boundary position moves slower [67].

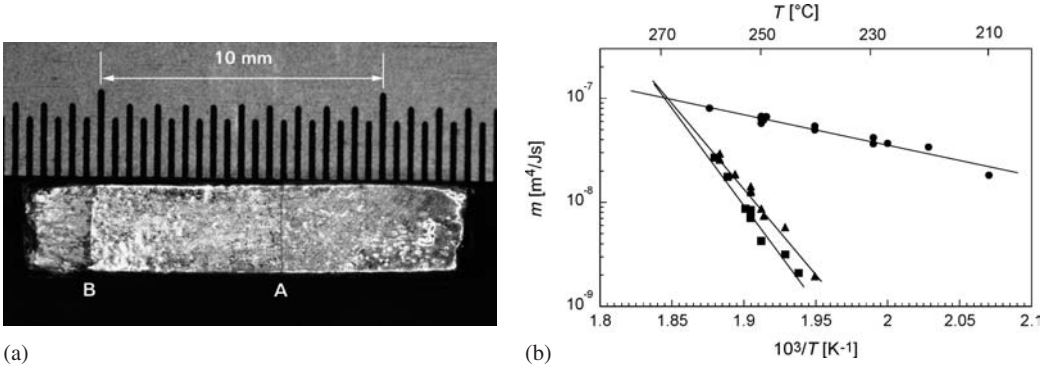

(a) (b)

Fig. 16. (a) Grain boundary displacement in a bismuth bicrystal (from position A to position B) after annealing for 180 s at 252 °C in a magnetic field of 20.45T [62] and (b) temperature dependence of the mobility of a 90° <112> symmetrical (●) and asymmetrical (▲, ■) boundaries in Bi-bicrystals, moving in opposite directions [30]. Trigonal axis in the growing grain parallel (▲) or perpendicular (■) to the growth direction.

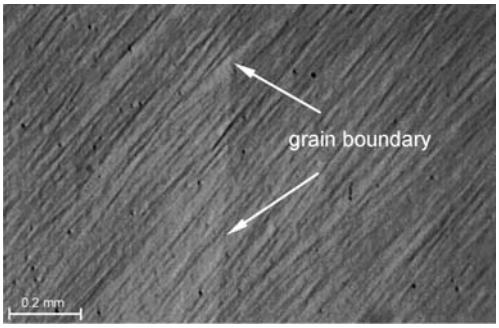

(a)

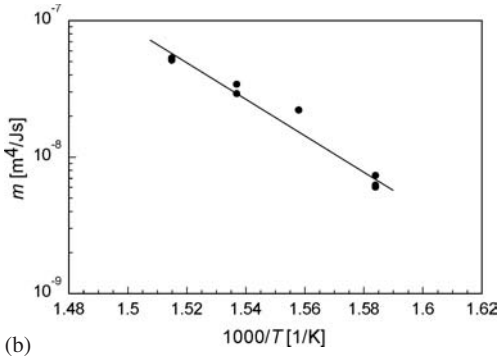

(b)

Fig. 17. Motion of a 47.2° <10$\bar{1}$0> grain boundary in a field of 25T at 370 °C in a zinc-bicrystal (a) as recorded by the polarization microscopy probe and (b) temperature dependence of the boundary mobility; the measured activation enthalpy of boundary motion amounts to 1.13 eV [70].

Figure 17a depicts the surface of a Zn-bicrystal containing a 47.2° < 10$\bar{1}$0> grain boundary as observed by employing the recently designed microscopy probe for in-situ observations and recordings of grain boundary migration in high magnetic fields [70]. Due to the orientation contrast between adjacent grains the grain boundary position is distinctly seen as a vertical line in the middle of the image. During post-processing the images are analyzed with respect to grain boundary displacement. The velocity of the steady-state boundary motion for each temperature could be calculated and the temperature dependence of the grain boundary mobility can be determined (Fig. 17b).

10. Mechanically driven motion of <100> tilt grain boundaries in Al coupled to shear deformation

Low angle grain boundaries are known to consist of periodic arrangements of dislocations. In earlier investigations in the 1950 by Washburn and Parker [9], Li et al. [10] and Bainbridge et al. [11] on Zn bicrystals, it was proved that low angle tilt grain boundaries respond to an applied mechanical stress by a displacement perpendicular to the boundary plane. According to the edge dislocation structure of such boundaries, their motion under mechanical stress was confirmed to be coupled to a shear deformation, which is observed in bicrystals with planar boundary as a tangential translation of the adjoining grains. Later Fukutomi et al. [71–73] also reported that high angle boundaries with low Σ CSL orientation relationships in Zn and Al bicrystals can be moved by an applied shear stress, which causes a shape change of the bicrystal. Similar behavior was observed by Yoshida et al. [74] for Σ11 boundary in cubic ZrO_2 bicrystals. The grain boundary motion coupled to a lateral grains translation was also investigated by Suzuki and Mishin [75] in a computer simulation study of <100> tilt grain boundary motion in Cu.

Recently, the stress induced boundary migration was experimentally investigated on aluminium bicrystals which contained symmetrical <100> tilt grain boundaries with misorientation angles in the entire misorientation range (0°–90°) [76–79].

The results revealed that stress induced boundary migration and the associated shear deformation is not confined to low angle and some low Σ high angle boundaries, but also occurs for all high angle <100> tilt boundaries. As a matter of fact motion in this fashion is a typical response of the boundary to the applied shear stress. Figure 18 depicts the coupled boundary motion for 66.6° <100> tilt boundary as apparent from the marking lines on the surface of the bicrystal and the shape change of the specimen. Furthermore, the experiments showed that in similarly loaded bicrystals boundaries with $\theta < 31°$ and $\theta > 36°$ move in opposite directions.

A coupling between boundary migration normal to its plane and the lateral translation of grains can be described by a ratio of corresponding rates [80] $\beta = v_{\|}/v_n = s/d$, (Fig. 18) where $v_{\|}$ and v_n are the lateral translation rates and the boundary velocity, respectively. The ratio β is referred to as the coupling factor.

The values of the coupling factor averaged over all investigated specimens of the respective bicrystal are given in Fig. 19. Since boundaries with $\theta < 31°$ and $\theta > 36°$ migrate

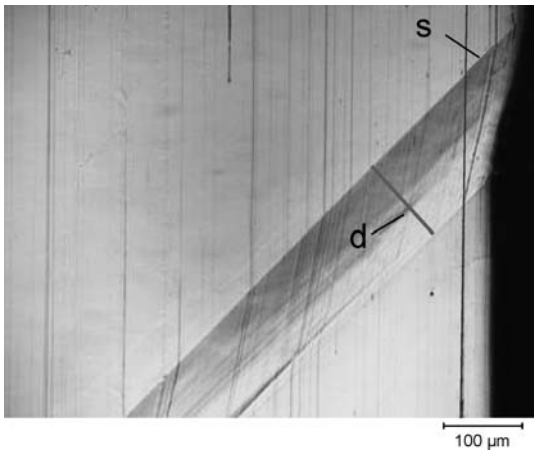

Fig. 18. Coupling between grain boundary migration and shear deformation for a 66.6° <100> symmetrical tilt boundary after 170 min annealing at 355 °C under a tensile stress of 0.26 MPa [78]. The coupling factor β was determined as a ratio of the lateral grains translation s to the normal boundary displacement d.

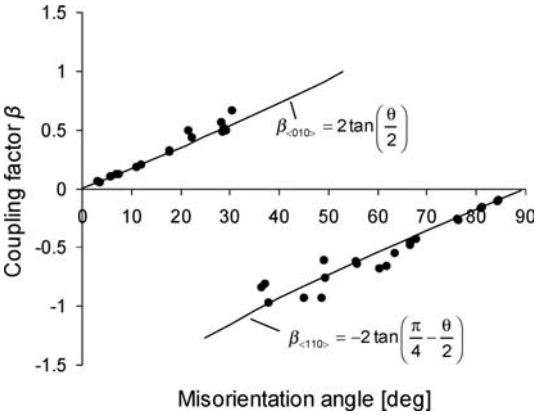

Fig. 19. Misorientation dependence of measured (points) and calculated (lines) coupling factors for investigated <100> symmetrical tilt grain boundaries [79].

in opposite directions, the corresponding values of β are different in sign.

It has been shown [81] that due to the 4-fold symmetry around the <100> axis in cubic crystals, for low angle <100> tilt boundaries there are two branches of the misorientation dependence of β. For slip of dislocations with $\boldsymbol{b}$ = a <010> on {001}

$$\beta_{<010>} = 2\tan\left(\frac{\theta}{2}\right) \tag{14}$$

while for slip on {110} with $\boldsymbol{b} = \frac{a}{2}$<110>

$$\beta_{<110>} = -2\tan\left(\frac{\pi}{4} - \frac{\theta}{2}\right) \tag{15}$$

A recently developed model of coupled boundary motion by Cahn et al. [82], based on an analysis of the Frank–Bilby equation of the dislocation content of grain boundaries, predicts a coupling factor between normal and lateral motion according to Eqs. (14) and (15) for any grain boundary, no matter whether low or high angle.

As seen in Fig. 19, there is excellent agreement between the experimental data and the coupling factors calculated according to Eqs. (14) and (15). The current results, therefore, prove that although in high angle boundaries the structural dislocations can not be resolved, the Frank–Bilby equation still applies. The experimentally measured coupling factors for stress induced tilt boundary migration comply perfectly with the respective dislocation mechanics.

The experiments revealed that boundary migration under an applied mechanical stress is thermally activated and that its kinetics follow an Arrhenius type temperature dependence (Eq. (3)). The temperature dependence of grain boundary mobility was measured in the temperature range between 280 °C and 450 °C, and the corresponding activation parameters were determined. The measured activation enthalpy scatters within the range between 1.0 and 1.6 eV (Fig. 20). For low angle boundaries ($\theta < 20°$ und $\theta > 70°$), however, the scatter of activation enthalpy values is less pronounced than for high angle boundaries ($20° < \theta < 70°$). The average value of H for low angle boundaries amounts to about H = 1.4 eV what is very close to that of bulk self diffusion in Al (H_{SD} = 1.47 eV [83]).

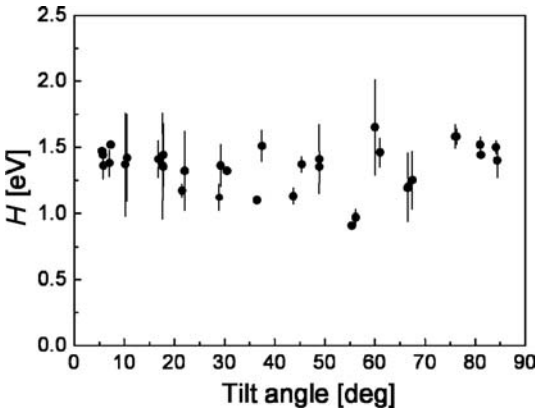

Fig. 20. Activation enthalpy of the stress induced migration of symmetrical <100> tilt grain boundaries [79].

11. Grain boundary excess free volume

The grain boundary excess free volume (BFV) is one of fundamental thermodynamic parameters of interfaces. Whereas the derivative $\left(\frac{\partial\gamma}{\partial T}\right)_P$ (γ – interface free energy) reflects the reaction of the interface on a temperature change, the derivative $\left(\frac{\partial\gamma}{\partial P}\right)_T$ describes the reaction to the applied external pressure.

It determines the grain boundary diffusivity, the mobility, and to a certain extent, grain growth inhibition by vacancy generation, it affects the stability and the kinetics of grain growth of polycrystals under high pressures. The value of the BFV determines the driving force to "squeeze" a grain boundary out of a polycrystal. On the other hand the BFV influences grain growth and other process connected to the generation of vacancies [84, 85]. Unfortunately, up to now we are forced be content with the results of computer simulations, which, in turn, are strictly limited to grain boundaries in the vicinity of special misorientations [86–90]. Some experimental attempts have been undertaken to determine the BFV [91–93].

The general-purpose and thermodynamically correct way to determine grain boundary excess volume was put forward in [93–95]. The approach is based on the fundamental difference between grain boundary and interphase: for the system with a grain boundary the number of degrees of freedom is by one greater than for an interphase. Therefore, for a system with a grain boundary all differentials on the right-hand side of Gibbs adsorption equation are independent:

$$\mathrm{d}\gamma = -s^{\mathrm{s}}\,\mathrm{d}T - \sum_{i=1}^{k} \Gamma_i\,\mathrm{d}\mu_i \tag{16}$$

where s^{s} and v^{s} are the entropy and the volume of the surface, Γ_i and μ_i are the adsorption and chemical potential of the ith component, T is the temperature.

Due to the additional degree of freedom a number of unique possibilities arise. In particular, one can consider adsorption in a one-component system, which can be called as an auto adsorption Γ_0:

$$\mathrm{d}\gamma = -s^{\mathrm{s}}\,\mathrm{d}T - \Gamma_0\,\mathrm{d}\mu \tag{17}$$

Of course, there is no sense in considering such a problem for an interphase, inasmuch as at constant temperature such a system is completely determined. The proposed method was realized in specially grown tricrystals where the triple junction is formed by two high angle grain boundaries GB1 and GB2 with equal grain boundary surface energy $\gamma_1 = \gamma_2 = \gamma$ (Fig. 21). The third grain boundary has to be a low angle grain boundary whose surface energy γ_3 can be calculated either according to the Read and Shockley approach or by direct computer simulation.

As it was shown in [93–95] for the system with low angle twist grain boundary the relation for BFV reads as:

$$V_{\mathrm{gb}}^{\mathrm{ex}} = \gamma_3 \frac{\sin\theta}{2\cos^2\theta}\frac{\partial\theta}{\partial P} \tag{18}$$

In other words, the problem is reduced to the experimental measurement of the pressure dependence of the contact angle θ.

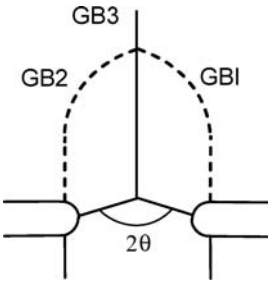

Fig. 21. Grain boundary geometry to determine the BFV: the grain boundary system with triple junction attains an equilibrium configuration at the notches introduced from the lateral surfaces of the tricrystal [95].

The experiments at 630 °C and under a hydrostatic pressure up to 14 kbar made it possible to measure the pressure dependence of the surface tension γ (Fig. 22) [95, 96].

The equilibrium vertex angle θ was measured for a grain boundary system of two 40° <111> tilt grain boundaries as GB1 and GB2 and an 80° <111> tilt boundary as GB3, which, due to crystal symmetry 80°<111> corresponds to −40° <111>, and the grain boundary energy of GB3 should be the same as the energy of GB1 and GB2. The measured angle was about 120° in the whole pressure range and, what is of importance $\left(\frac{\partial\theta}{\partial P}\right)_T = 0$ as was to be expected.

Below are presented the value of the BFV for 40° <111> tilt grain boundary and 39° <110> tilt grain boundary extracted from the experimental data [95, 96]

<110>

$$\Gamma_0 = -\Omega_s^{-1}\left(\frac{\partial\gamma}{\partial P}\right) = -1.35\cdot 10^{-5}\ \mathrm{mol/m^2} \qquad (19)$$

$$V^{ex} = -\Gamma_0\Omega_a = 1.35\cdot 10^{-10} \pm 0.6\cdot 10^{-10}\ \mathrm{m^3/m^2}$$

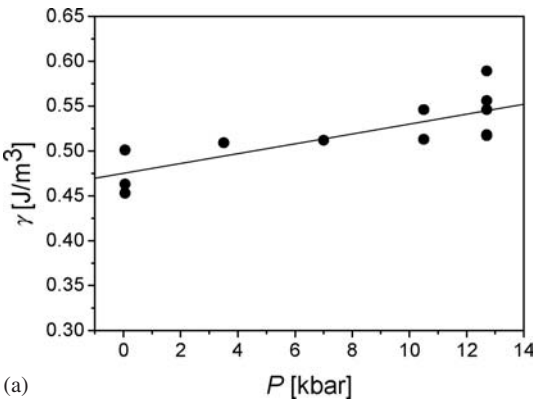

(a)

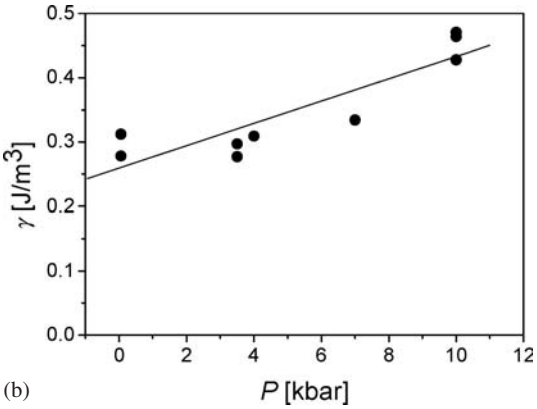

(b)

Fig. 22. Pressure dependence of grain boundary surface tension (a) for 40° <111> tilt boundary and (b) for 39° <110> tilt boundary in Al [95, 96].

<111>

$$\Gamma_0 = -\Omega_a^{-1}\left(\frac{\partial\gamma}{\partial P}\right) = -0.55\cdot 10^{-5}\ \mathrm{mol/m^2} \qquad (20)$$

$$V^{ex} = -\Gamma_0\Omega_a = 0.55\cdot 10^{-10} \pm 0.13\cdot 10^{-10}\ \mathrm{m^3/m^2}$$

The corresponding expression for grain boundary surface tension is given by the relationship

$$\gamma_b = \gamma_{b0} + \left(\frac{\partial\gamma_b}{\partial P}\right)_T P \qquad (21)$$

One might expect that such a difference in the excess grain boundary volume for different grain boundaries can play an important role in grain microstructure evolution in the course of grain growth, in particular in thin films on the substrate and especially in nanocrystalline systems.

12. Kinematics of connected grain boundaries

The classical concepts of grain growth in polycrystals are based on a dominant role of grain boundaries. This is reflected by the well known von Neumann–Mullins relation.

$$\frac{dS}{dt} = -A_b\left(2\pi - \frac{n\pi}{3}\right) = \frac{A_b\pi}{3}(n-6) \qquad (22)$$

where A_b is a reduced grain boundary mobility, n is the number of triple junctions for each respective grain, i.e. the topological class of the grain. This relation which forms the basis for practically all theoretical and experimental investigations as well as computer simulations of microstructure evolution in 2D polycrystals in the course of grain growth [97, 98] is based on three essential assumptions, the most important of which is the assumption relevant to grain boundary triple junctions: they do not affect grain boundary motion, their role in grain growth is reduced to maintain the thermodynamically prescribed equilibrium angles at the lines where boundaries meet. This assumption is a mere hypothesis and needs to be checked experimentally. For this it is necessary to measure the triple junction mobility. The theoretical approaches and experimental techniques which make it possible to study the steady-state motion of grain boundary systems with triple junction were put forward and developed in [99–103]. As shown in [99–103], the model grain boundary systems (Fig. 23) can move in steady-state, and the analysis of their motion permits us to understand the influence of the finite mobility of a triple junction on the migration of grain boundaries.

It was shown that the behavior of a grain boundary system with triple junction is determined by the dimensionless criterion $= \frac{m_{tj}a}{m}$, where m_{tj} is the triple junction mobility, and a is the grain size:

$$\Lambda = \frac{m_{tj}a}{m_b} = \frac{2\theta}{2\cos\theta - 1}, \quad n < 6 \qquad (23)$$

$$\Lambda = \frac{m_{tj}x_0}{m} = -\frac{\ln\sin\theta}{1-2\cos\theta}, \quad n > 6 \qquad (24)$$

If a triple junction is mobile and does not drag grain boundary motion, the criterion $\Lambda \gg 1$ and $\theta = \pi/3$ i.e. the

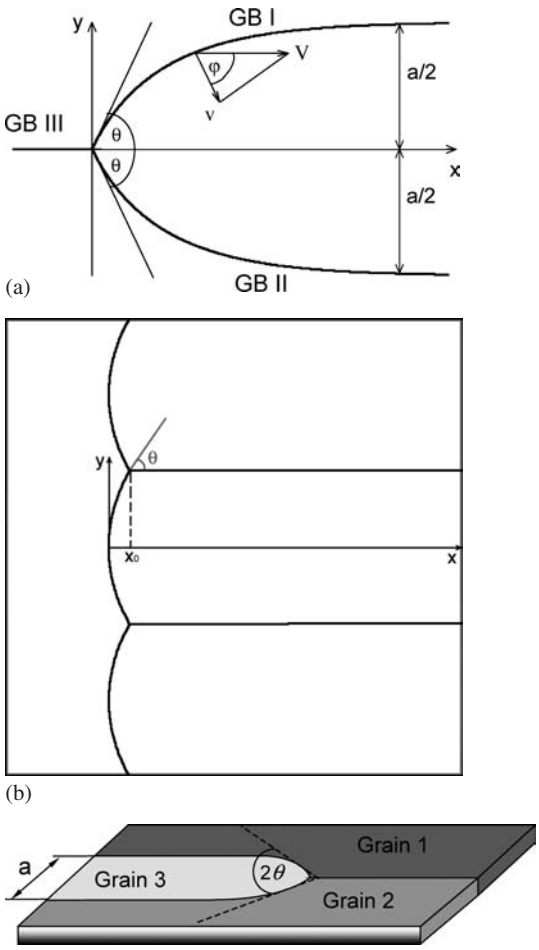

Fig. 23. Configuration of grain boundaries at a triple junction during steady state motion for (a) $n < 6$ and (b) $n > 6$; (c) – top view of the tricrystal of the configuration with $n < 6$.

equilibrium angular value at a triple junction in the uniform grain boundary model. In contrast, however, when the mobility of the triple junction is relatively low (strictly speaking, when $m_{tj}a \ll m$) then $\theta \to 0$ for $n < 6$ and $\theta \to \pi/2$ for $n > 6$. It should be stressed that the angle θ is strictly defined by the dimensionless criterion Λ, which, in turn, is a function of not only the ratio of triple junction and grain boundary mobility, but of the grain size as well.

Experimental investigations were carried out for the grain boundary configuration shown in Fig. 24 in specially grown tricrystals of Al and Zn [38, 100–104]. It was demonstrated that the shape of the moving grain boundary system agrees very well with the shape predicted by the theory [38, 101, 102] and the vertex angle θ at the triple junction can deviate distinctly from the equilibrium value, when a low mobility of the triple junction hinders the motion of the grain boundaries (Fig. 25). In fact, a transition from triple junction kinetics to grain boundary kinetics was observed. Experiments revealed that triple junctions do possess a finite mobility. Moreover, the extent of the changes in the angle θ and criterion Λ are such that they do not allow their explanation by thermodynamic factors and there are no doubts in the kinetic nature of the phenomena.

Molecular dynamics simulation studies of the migration of grain boundaries with triple junctions confirm that the triple junction mobility is finite and can be sufficiently small to limit the rate of grain boundary migration [105, 106]. The analytical solutions and the analysis of grain boundary motion serve as a theoretical background of the studies discussed. The static-equilibrium-grain boundary triple junction angles and the dynamic triple junction angles were measured as a function of grain size, grain boundary misorientation and direction of migration. In most cases, the static and dynamic triple junction angles were observed to be nearly identical. However, substantial deviations between the two were observed for low Σ boundary misorien-

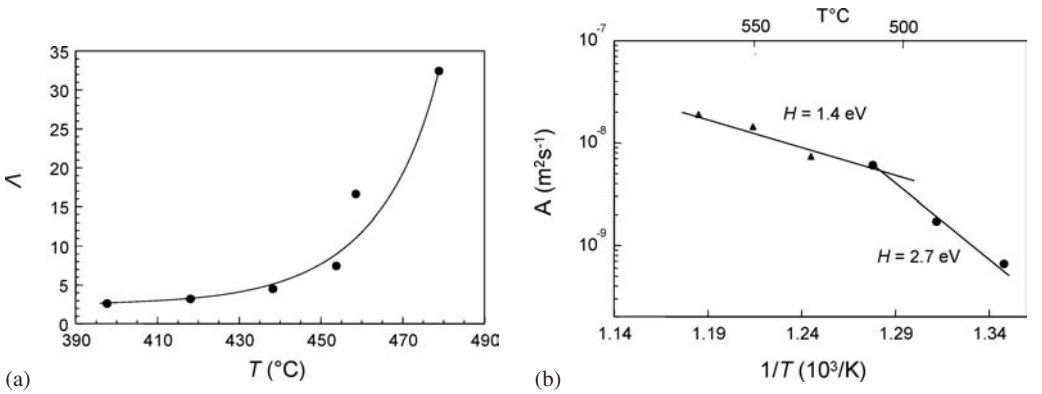

Fig. 24. Temperature dependence of the criterion Λ (a) and of triple junction (●) and grain boundary mobility (▲) for <111> tilt grain boundary system in pure Al [103].

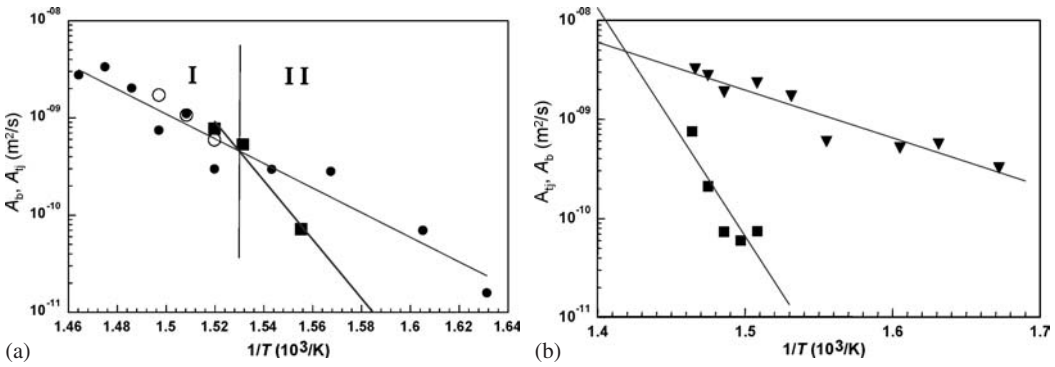

Fig. 25. Temperature dependence of reduced grain boundary mobility A_b(solid circles) and reduced triple junction mobility A_{tj} (solid squares) for the system <10$\bar{1}$0> (a) and for the system <11$\bar{2}$0> (b): reduced grain boundary mobility A_b (solid triangles) and reduced triple junction mobility A_{tj} (solid squares) [104].

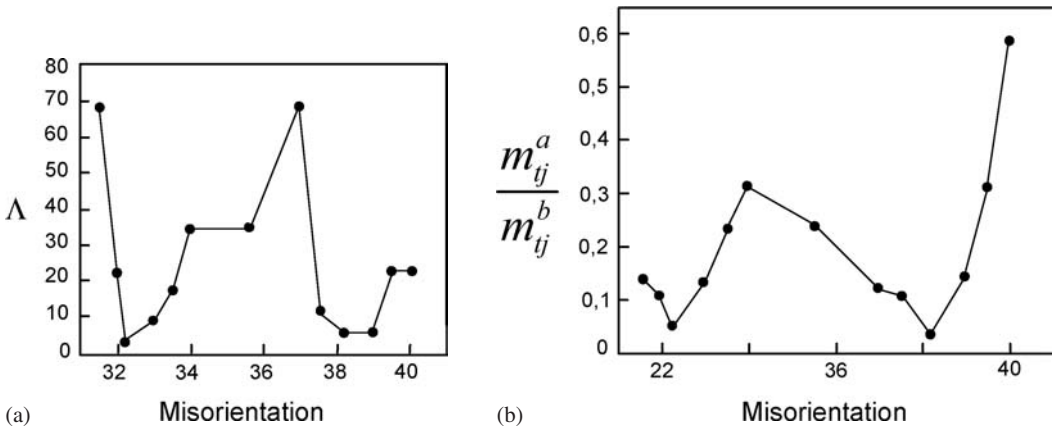

(a) (b)

Fig. 26. (a) The misorientation dependence of the criterion Λ obtained in the simulations with geometry given in Fig. 23a at $T = 0.3\ T_m$ and (b) the ratio $\frac{m^a_{tj}}{m^b_{tj}}$ of the triple junction mobility extracted for the simulation geometry shown in Fig. 23a (m^a_{tj}) and Fig. 23b (m^b_{tj}) [105].

tations (Fig. 26). Furthermore, the normalized triple junction mobility exhibits strong variations with boundary misorientation, with strong minima at low Σ misorientations. The triple junctions create substantial drag on grain boundary migration at these low mobility misorientations [106, 107]. One interesting feature of the results is that the triple junction mobility depends upon the direction that the triple junction migrates. Again, the normalized triple junction mobility was found to have significant dependence on direction of migration for the case of low Σ grain boundaries (Fig. 26).

Four topological elements compose a polycrystal: grains, grain boundaries, grain boundary triple junctions and quadruple points. The latter element of the microstructure is located at the point where four grain boundaries meet. The four grains assembly which admits a quantitative description was proposed in [108, 109] (Fig. 27). In such configuration, it is assumed that the motion of the triple lines in the system proceeds under the action of the triple line tension γ' and is assumed to occur in steady-state (which takes place if the shrinkage of the three-sided cross-section proceeds much more slowly than the displacement of the quadruple junction).

The dimensionless parameter describing the influence of the quadruple junction is given by

$$\Lambda_{qp} = -\frac{\ln\sin(\pi-\theta)}{1+3\cos\theta} = -\frac{\ln\sin\theta}{1+3\cos\theta} = \frac{m_{qp}\cdot x_0}{m_{tl}} \qquad (25)$$

where m_{qp} is the mobility of the quadruple point, x_0 is the grain size.

If the quadruple junction is perfectly mobile, then $\Lambda_{qp} \to \infty$ and $\theta \to 109.47^\circ$, which is the equilibrium angle. By the way, this angle is consistent with the dihedral angle of the honeycomb. In contrast, if the quadruple junction moves slowly and drags the migration of the triple lines then $\Lambda_{qp} \to 0$ and $\theta \to \pi/2$. It can be seen that from the Eq. (25) that the angle θ completely defined by the dimensionless parameter Λ_{qp} which, in turn, does not only depend on the triple line and quadruple junction mobilities but also on the grain size, x_0. It indicates that the effect of quadruple junctions increases with decreasing grain size.

13. 2D grain growth in the system of connected boundaries

As a matter of fact that grain boundary triple junctions do possess a finite mobility [38, 100–104]. This circumstance effects radically our understanding of the physics of grain growth. The rate of grain area change can be express as

$$\frac{dS}{dt} = -A_b[2\pi - n(\pi - 2\theta)] \qquad (26)$$

If the triple junction mobility is infinite the contact angle $\theta = \pi/3$ and the expression (26) will be transferred into the well known von Neumann–Mullins relation. However

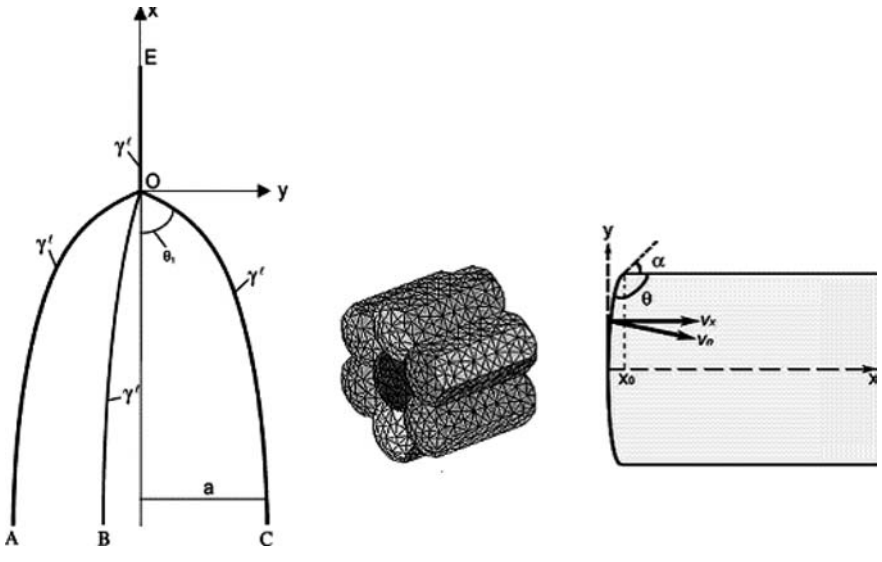

(a) (b) (c)

Fig. 27. (a) Four grain arrangements with four triple lines (OA, OB, OC, OE) and one quadruple point at O. The angle θ_1 is the vertex angle of a triple line at the quadruple junction, a is the (half) dimension of the grain bounded by the OA, OB and OC [108]; (b) The special grain assembly allows a steady-state motion of the quadruple points; (c) Shape of the grain boundaries and definition of the variables used for the derivation of the equation of motion) [109].

for $m_{tj} \neq \infty$ the parameter Λ is a function of θ and the rate of grain area change is a function of Λ as well. As it was shown in [108,1 10] the explicit forms for the dependency $\dot{S}(n, \Lambda)$ are:

$$\dot{S} = \frac{m_b \gamma_b \pi}{3}\left(n\frac{6+\sqrt{3}\,\Lambda}{2+\sqrt{3}\,\Lambda} - 6\right)$$

and (27)

$$\dot{S} = \frac{m_b \gamma_b \pi}{3}\left[n\left(1 - \frac{6}{\pi \Lambda B}\right) - 6\right], \quad B = -\frac{\sqrt{3}}{\ln \sin \pi/3}$$

for $n < 6$ and $n > 6$ respectively.

For $\Lambda \to \infty$ – boundary kinetics regime – Eq. (27) is identical with the classical von Neumann–Mullins relation. Accordingly for the topological class n^* of grains for which $\dot{S} = 0$

$$n^* = \frac{2+\sqrt{3}\,\Lambda}{1+\frac{\sqrt{3}}{6}\Lambda} \text{ for } n < 6 \quad \text{and} \quad n^* = \frac{6}{1-\frac{6}{\pi \Lambda B}} \text{ for } n > 6 \tag{28}$$

The quantitative variation of the rate of grain area change $\dot{S}$ on topological class n, which is a straight line for pure grain boundary kinetics undergoes the principal modification: this dependency is transformed to an area under the constraint of a finite triple junction mobility (Fig. 28). While for unconstrained grain boundary kinetics (infinite junction mobility) $\dot{S}$ is a function of n only, for a system with finite junction mobility $\dot{S}$ becomes a function of both n and Λ, $\dot{S} = \dot{S}(n, \Lambda)$ (Fig. 28).

For the first time it has been shown experimentally that due to triple junction drag there is no unique linear relationship between growth rate and the number n of grain sides, as proposed by the classical von Neumann-Mullins relation. The drag influence of the triple junctions causes the growth rate to depend not only on n but on the criterion Λ as well, i.e. $\dot{S}(n, \Lambda)$ [110, 111].

The discussed consequence afforded by the developed approach is probably the most significant one, however, it is worthy noting some more quantitative predictions made in [108, 110, 111]. It is seen that the drag effect of grain boundary triple junctions results in a change of the topological limit between the classes of shrinking and growing grains such that the limit decreases for shrinking grains but increases for growing grains. This behavior $n^*(\Lambda)$ (Eq. (28)) becomes obvious from Fig. 29 where the cases $n < 6$ and $n > 6$ are distinguished as $n_L^*(\Lambda)$ and $n_H^*(\Lambda)$, respectively. Grains are neither capable of growing nor shrinking in the intermediate situation that manifests itself in the dependency $n^*(\Lambda)$

- Under triple junction kinetics grains should be bordered by flat boundaries, i.e. straight lines in 2D.

Under triple junction kinetics a system of polygons tends to transform to a system of equilateral polygons. The only exception is the triangle which will collapse without transforming into a regular polygon. Figure 30 pictures the dependency "mean grain topological class – mean grain area" extracted from the grain growth in 2D Al foils [112,

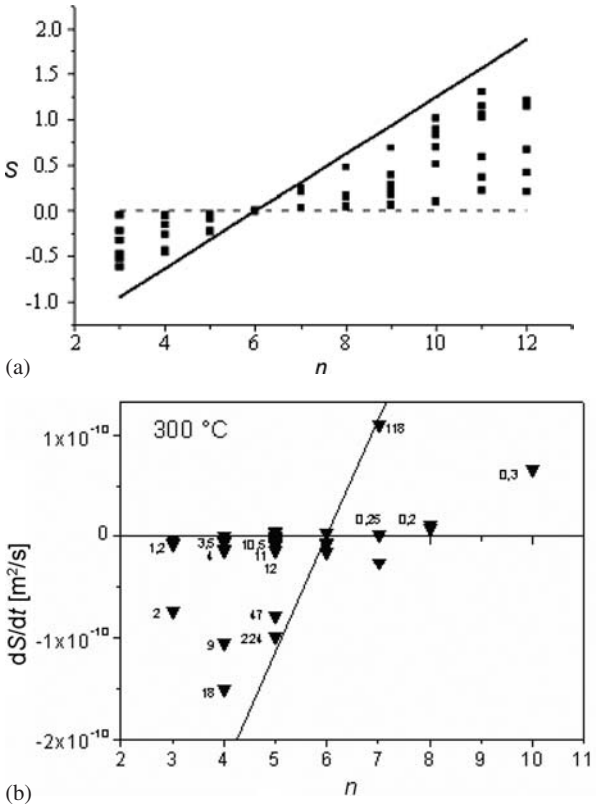

Fig. 28. (a) $\dot{S}$ as function of n for $0.1 < \Lambda < 10$. Solid squares are the results of computer experiments, the line represents the von Neumann–Mullins relation (computer simulation) [111]. (b) Rate of grain area change dS/dt versus topological class n of a grain for grain growth at 300 ° in 2D Al sheet. The values of Λ are given next to the data point [110].

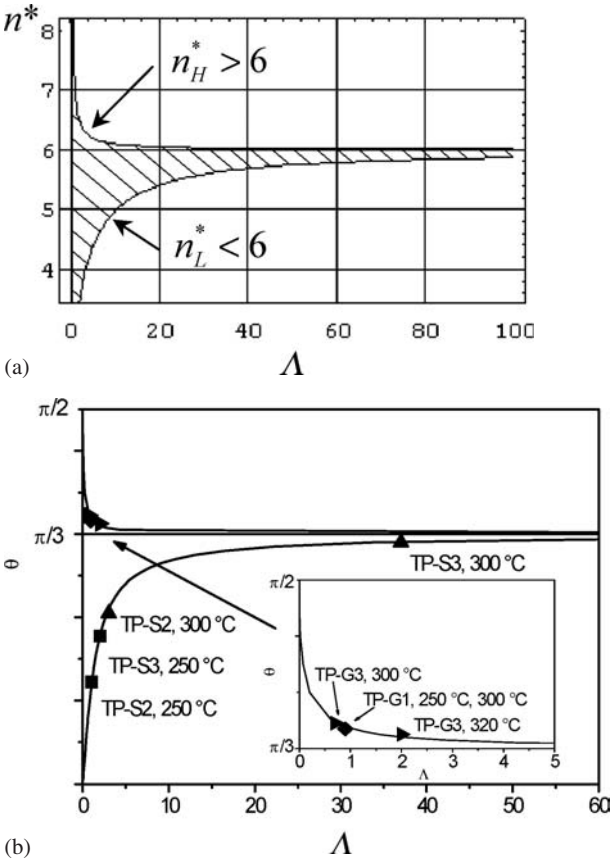

Fig. 29. (a) Dependence of n_H^* and n_L^* on Λ (computer simulation [111]); (b) Vertex angle θ versus criterion θ (grain growth in 2D Al sheet) [110].

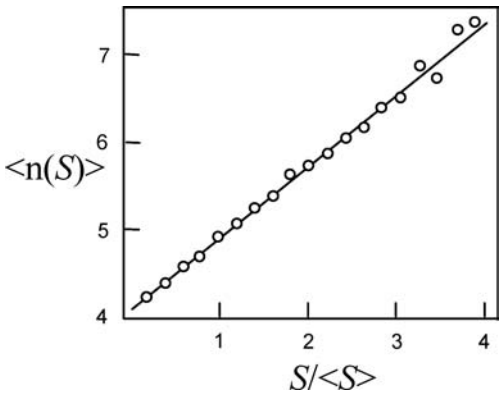

Fig. 30. The Dependence "mean grain topological class – mean grain area", extracted from the experimental data of grain growth in 2D Al foils [112, 113].

113]. As can be seen $n = 4$ is the smallest topological class to shrink in a stable manner.

- For triple junction kinetics the rate of grain area change can be described as $\langle S \rangle \sim t^2$. Such a behavior was observed in [114].

It should be stressed that the since the value of the dimensionless criterion Λ decreases with the reduction of the grain size the mentioned regularities come into particular prominence for fine grained and nanocrystalline systems.

An additional point to emphasize is that since the part of the grains has vanished in the course of the grain growth the influence of the triple junctions persists even in the polycrystals with rather large grain size.

14. 3D grain growth in the system of connected boundaries

The success of von Neumann–Mullins relation which established the interplay between the topology of the grain and the rate of grain area change for 2D polycrystal inspired the scientists to search the 3D analogy of such an interrelation [115–122]. The models considered by Mullins, Hilgensfeldt and Glicksman and Rios were derived under the assumption that the volume evolution of grains within a topological class can be accurately described by an average value for the whole class. Cahn [115] expressed the integral curvature of the surfaces of 3D convex grains as a function of the average caliper diameter. On the same note, MacPherson and Srolovitz [121] demonstrated that the integral curvature of any closed domain is given by:

$$\int_{\partial D} H \, \mathrm{d}A = 2\pi \left(L(D) - \frac{1}{6} e(D) \right) \tag{29}$$

where H is the mean curvature, $L(D)$ is the mean width of the domains. The mean width is the natural linear measure of a domain and for a convex grain is equal to the mean caliper radius.

The developed 3D computer model has been validated for several applications [109] and reflects the physics underlying the grain growth process. The proposed special configuration manifests a steady-state motion of the grain boundaries and junctions of the polycrystal. It was found that the behavior of the system is determined by the dimensionless parameter Λ_{qp}, which is related to the quadruple junction mobility. The results show that a finite quadruple junction mobility can slow down grain growth. However, the simulations also demonstrated that a finite triple line mobility hinders grain growth, even more effectively. In part, it was quantitatively considered which grain boundary junction is more efficient in grain growth dragging. For intermediate values of Λ_{tj}, Λ_{qp} the differences in $\dot{V}(\Lambda)$ are markedly pronounced, because $\dot{V}(\Lambda)$ is more sensible to a change of Λ_{tj} than of Λ_{qp} (Fig. 31) [109, 123]. In essence, triple lines drag grain-boundary motion more effectively than quadruple junctions contrary to predictions of Brechet and co-workers [124].

It has been shown that computer simulations with a 3D vertex model agree very well with the analytical results of the different considered approaches, in particular, the simulations showed a good accordance with the Cahn–MacPherson–Srolovitz relation calculated from only the geometrical characteristics of all the grains of the accounted polycrystal. **This relation points out that, contrary to von Neumann–Mullins relation, grains with the same**

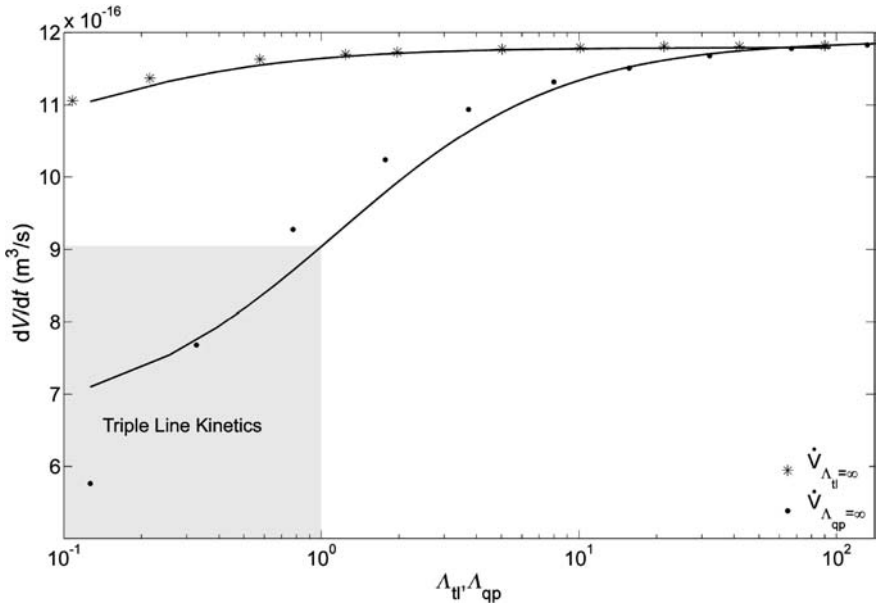

Fig. 31. Volume change rate, for (*) Λ_{qp} is varied while Λ_{tl} is held infinite and for (●) Λ_{tl} is varied whereas Λ_{qp} is held infinite [123].

topological class may have different growth rates and, thus, there is no a general relation between growth rate and topological class for individual grains. Nevertheless, relations that accurately describe the mean growth rate of grains within the same class are helpful because such relations can be used to derive general properties of polycrystals and can assist in a better understanding of the process of grain growth from a statistics point of view.

It should be stressed also that such good agreement between analytical description and experiment (computer simulation) was observed **only** for infinite mobility of grain boundary junctions [123].

The examination of this problem for different (non-infinite) values of triple line and quadruple junction mobility have shown that in all cases, an **essential deviation** between the experiment and analytical description was found [123].

In essence, if the objective of a study is the general growth behavior of grains within a topological class, Mullins, Glicksman – Rios and Hilgenfeldt approaches are excellent options. However, since the Cahn – MacPherson – Srolovitz expression can be considered as an exact expression for the grain growth of individual grains as a function of only geometrical characteristics, it can be used for the theoretical study of more fundamental phenomena such as grain boundary motion in small grain assemblies.

The approach which makes it possible to extract the mobility of grain boundary junctions from the data of the grain growth was put forward in [125]. As was shown earlier, Eq. (30) defines the different types of grain growth kinetics in polycrystals.

$$V = \frac{m_b \gamma_b \kappa}{1 + \frac{1}{\Lambda} + \frac{1}{\Lambda_{qp}}} \tag{30}$$

The first one is the well-known grain boundary kinetics: $\frac{1}{\Lambda}, \frac{1}{\Lambda_{qp}} \ll 1$, the velocity V is proportional to the grain boundary curvature, and the mean grain size increases in proportion to the square root of the annealing time: $V = \frac{d<R>}{dt} \sim \frac{1}{<R>}$, $<R> \sim \sqrt{t}$. If grain boundary motion is controlled by the mobility of triple junctions $\left(\frac{1}{\Lambda} \approx 1 \text{ and } \frac{1}{\Lambda} \gg \frac{1}{\Lambda_{qp}}\right)$, the velocity V is constant: $V = \frac{d<R>}{dt} = \text{const.} \Rightarrow <R> \sim t$. Finally, if the mobility of the quadruple junctions (points) determines the motion of the grain boundary system $\left(\frac{1}{\Lambda_{qp}} \gg 1 \text{ and } \frac{1}{\Lambda_{2qp}} \gg \frac{1}{\Lambda}\right)$ the velocity V is proportional to the radius of curvature: $V = \frac{d<R>}{dt} \sim <R> \Rightarrow <R> \sim e^t$. Under grain boundary kinetics we observe the classical grain growth kinetics, which is to hold for rather large grains. The time dependency of the mean grain size determined by triple junction kinetics ($<R> \sim t$) was observed for grain growth in ultrafine grained and nanocrystalline materials [126 – 128].

The experimental data of the grain growth in nanocrystalline Pd not only demonstrate the possibility of such a kinetic regime but allow us to extract the grain boundary quadruple junction mobility [128]. Moreover, using the approach described it is possible to extract the kinetic parameters of grain growth inhibited by boundary junctions. For example, the reduced mobility of quadruple junctions in nanocrystalline Pd [128] can be estimated as $m_{qp}\gamma_b = 2 \cdot 10^{-5}\ s^{-1}$.

14. Computer simulation of grain boundary motion

In spite of large efforts undertaken to develop the technique of the measurements and observation of grain boundary migration and of obvious success in this area the mechanism of grain boundary motion is still "terra incognita". It seems that the only way to understand this phenomenon is to utilize the computer simulation, namely the molecular-dynamics simulation. There are some successful works in this area. Jhan and Bristowe [129, 130] confirmed the concept of a cooperative shuffle mechanism of grain boundary motion, which was supported by Babcock and Balluffi's observation [131]. A curved grain boundary which moves under a constant driving force was presented by Upmanyu et al. [132] and used in the computer simulation the half-loop grain boundary that allowed study the motion of a curved grain boundary under a constant driving force.

A methodology of the observation and measurements of a planar boundary under a constant driving force in a wide range of misorientation angle was put forward in [133 – 135]. **The analysis reveals that in absolutely pure materials high-angle grain boundaries move by a collective shuffle mechanism, while low-angle boundaries do move by a dislocation based mechanism.** The important conclusion concerns the compensation effect. The main relation of the compensation effect – the linear dependence between the activation energy and the logarithm of the pre-exponential factor – was observed in the computer experiments.

It was proved that grain boundary self-diffusion remained almost identical for stationary and moving grain boundaries, fact which was experimentally established in the classical works of Gust and co-workers [136, 137]. Of course, the computer simulation gives the possibility studying it in greater detail; namely, it was recognized that grain boundary self-diffusion via vacancies remains the same for non-driven and driven grain boundaries [135]. Finally, it was stressed that grain boundary migration cannot be understood in terms of grain boundary self-diffusion, since **grain boundary migration and grain boundary self-diffusion are distinctly different processes**.

15. Kinetics of grain growth inhibited by vacancy generation

It is very common in materials science that vacancies are generated as a by-product of a kinetic process. The excess free volume the system has to get rid of in such kinetic processes is released as vacancies which have to be accommodated by the crystal bulk. The supply of vacancies in the course of grain growth may produce a vacancy supersaturation in the bulk raising the Gibbs free energy G and producing a negative thermodynamic force. As can be expected intuitively, particularly by analogy with the Le Chatelier principle, this thermodynamic force will resist grain boundary migration. This idea was put forward and formed the

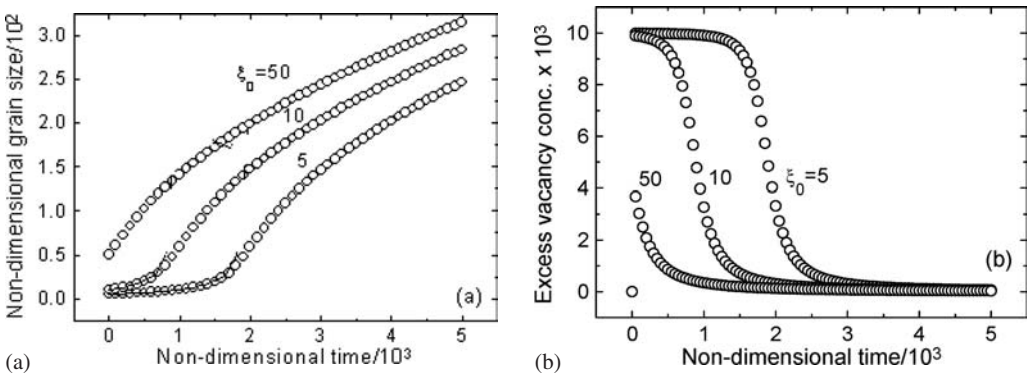

Fig. 32. Dependence of (a) non-dimensional grain size $\xi = \bar{R}/d$ and (b) excess vacancy concentration on the non-dimensional time $\bar{t}$ ($\bar{t}$ is measured in the units of d^2/D_v) [85].

basis of the approach considered in [84, 85, 138–140]. The general equation which expressed how the driving force is distributed between the dissipation due to the drag forces and the vacancy sub-system was derived.

Numerical solutions for a broad range of parameters has shown that for sufficiently small initial grain size $\xi_0 = R_0/d$ (R is the average grain size, radius, d is the average spacing between vacancy sinks) the grain growth uninhibited by vacancies is preceded by an incubation time during which the growth rate is substantially reduced, the time dependence of the grain size exhibiting a plateau-like behavior (Fig. 32a). For large values of ξ_0 no incubation time is observed. The incubation time is defined as the time at which the grain growth rate is a maximum. This time corresponds to the termination of the plateau-like behavior and a transition to uninhibited, parabolic grain growth. Over the incubation time, the vacancy concentration stays at an approximately constant, increased level (Fig. 32). Numerical results show the incubation time is inversely proportional to ξ_0.

The results obtained in [85, 138–140] have a direct relationship to the grain growth and stability of nanocrystalline materials. In particular, the condition for the vacany-induced stabilization of nanocrystalline materials was obtained [85].

As was shown in [85], for very small initial grain size mean grain size $\bar{R} \sim t$.

It is worthy of note that the main area of the approach discussed are the processes in fine grained and nanocrystalline materials. Specifically, the linearity between mean grain size and the annealing time was observed experimentally for grain growth in nanocrystalline iron [114].

The approach was applied to grain growth in thin films, to grain refining due to vacancy supersaturation.

16. Final remarks

It is difficult to overestimate the impact of grain boundaries and grain boundary junctions on the properties of the polycrystalline materials and kinetics of the processes with their participation. However, there is the area of scientific exploration and industrial feasibility where the role of grain boundaries and especially connected grain boundaries is decisive. The case in point is the ultra fine grained and nanocrystalline materials. Since the major distinctive feature of nanostructures is a large density of grain boundaries, all aspects considered above directly apply to the evolution of grain microstructure in these materials and its thermal stability that in turn defines their properties.

As has been shown in recent years, the properties and especially behaviour of the grain boundary net in polycrystals cannot be predicted from the properties of individual grain boundaries only, i.e. the role of grain boundary junctions in microstructure development should be taken into account. For fine grained and nanostructured materials the influence of boundary junctions may be crucial, since the smaller the grain size the greater is the effect of junctions on grain growth due to their limited mobility.

One of the existing challenges is the measurement of the free energy (line tension) of grain boundary triple junctions. The value of the triple junction energy becomes extremely important for modeling of microstructural development in nanostructured systems, since the junctions energy may constitute an essential fraction of the driving force of grain growth.

Furthermore, taking into account the essentially altered distribution of grain boundaries on their character, i.e. on their structure and excess free volume, the competitive adsorption of impurity atoms at grain boundaries and triple lines and the re-distribution of solutes between the boundaries and triple lines are inevitable for modeling the microstructure of fine grained polycrystals.

In recent years it has been recognized that plasticity in polycrystalline materials with severely reduced grain size is not necessarily carried out by dislocations, rather most likely is associated with grain boundary related processes such as grain boundary sliding, grain rotation and grain boundary motion. A number of experimental and modeling studies of the grain boundary mediated plasticity in nanostructured materials and of the boundary migration coupled to shear deformation have been performed quite recently. However, we still do not possess a comprehensive understanding of the respective fundamental mechanisms. Therefore, further simulations and experiments on bicrystals containing grain boundaries with well defined structure as well as on nanostructured polycrystals are required.

Due to a very high volume fraction of grain boundaries in nanostructured materials, the physical properties of these materials can probably be remarkably changed. As has been shown by Breger and Zhukhovitskii in the 1930s, the heat capacity c of the polycrystalline system with well-developed interfaces at low temperatures can be represented as a sum of the "bulk" c_v and "interface" c_i heat capacity

$$c = c_v + c_i = \alpha N_0 k \frac{T^3}{\theta^3} + \beta N_0 k \frac{T^2}{\theta^2} \qquad (31)$$

where $N_0 = (V/\Omega_a)N_A$, V is mean grain volume, N_A is Avogadro number, Ω_a is atomic volume, θ is Debye tem-

perature, α and β are numerical coefficients. It can be seen that for Al polycrystal ($\theta = 428$ K) with the grain size of 50 nm the specific heat at $T = 4$ K should be larger than for the polycrystal with grains of conventional size by a factor of three.

Also, it has been shown in the 1970s that the critical temperature of the superconductivity of polycrystals may be a little larger than this of a single crystal. For nanostructured materials this effect might be expected to be significant.

References

[1] U. Czubayko, D.A. Molodov, B.-C. Petersen, G. Gottstein, L.S. Shvindlerman: Meas. Sci. Technol. 6 (1995) 947.
[2] D. Mattissen, D.A. Molodov, G. Gottstein, L.S. Shvindlerman, in: G. Gottstein, D.A. Molodov (Eds.), Recrystallization and Grain Growth, Springer, New York (2001) 421.
[3] D.M. Kirch, A. Ziemons, T. Burlet, I. Lischewski, X. Molodova, D.A. Molodov, G. Gottstein: Rev. Sci. Instrum. 79, 043902 (2008).
[4] P.J. Konijnenberg, A. Ziemons, D.A. Molodov, G. Gottstein: Rev. Sci. Instrum. 79, 013701 (2008).
[5] C.G. Dunn, F.W. Daniels, M.J. Bolton: Trans. AIME 185 (1949) 708.
[6] B.B. Rath, H. Hu, in: H. Hu (Ed.), The Nature and Behavior of Grain Boundaries, Plenum Press, N.Y. (1972) 405.
[7] R.C. Sun, C.L. Bauer: Acta metall. 18 (1970) 635.
[8] W.W. Mullins: Acta Metall. 4 (1956) 421–432.
[9] J. Washburn, E.R. Parker: Trans. AIME 194 (1952) 1076–1078.
[10] C.H. Li, E.H. Edwards, J. Washburn, E.R. Parker: Acta Metall. 1 (1953) 223.
[11] D.W. Bainbridge, C.H. Li, E.H. Edwards: Acta Metall. 2 (1954) 322.
[12] W.T. Read, W. Shockley: Phys. Rev. 78 (1950) 275.
[13] D.A. Molodov, V.A. Ivanov, G. Gottstein: Acta Mater. 55 (2007) 1843.
[14] M. Peach, J.S. Koehler: Phys Rev. 80 (1950) 436.
[15] J.W. Rutter, K.T. Aust: Acta Metall. 13 (1965) 181.
[16] D.A. Molodov, B.B. Straumal, L.S. Shvindlerman: Scripta Metall. 18 (1984) 207.
[17] V. Yu. Aristov, V.L. Mirochnik, L.S. Shvindlerman: Sov. Phys. Solid State 18 (1976) 137.
[18] V.G. Sursaeva, A.V. Andreeva, C.V. Kopezkii, L.S. Shvindlerman: Phys. met. metall. 41 (1976) 98.
[19] G. Ibe, K. Lücke: Recrystallization, Grain Growth and Textures, American Society for Metals, Metals Park, Ohio (1966) 434.
[20] G. Ibe, W. Dietz, A.-C. Fraker, K. Lücke: Z. Metallkd. 61 (1970) 498.
[21] G. Ibe, K. Lücke: Texture 1 (1972) 87.
[22] F.J. Humphreys, M. Hatherly: Recrystallization and Related Annealing Phenomena, Elsevier Science Ltd., Oxford (1995) 100.
[23] E. Nes, H.E. Vatne: Z. Metallkd. 87 (1996) 448.
[24] K. Lücke: Canadian Metallurgical Quarterly 13 (1974) 261.
[25] D.A. Molodov, U. Czubayko, G. Gottstein, L.S. Shvindlerman: Scripta Metall. Mater. 32 (1995) 529.
[26] D.A. Molodov, U. Czubayko, G. Gottstein, L.S. Shvindlerman: Acta Mater. 46 (1998) 553.
[27] V. Ivanov, D.A. Molodov, L.S. Shvindlerman, G. Gottstein: Mater. Sci. Forum 467–470 (2004) 751.
[28] M. Upmanyu, D.J. Srolovitz, L.S. Shvindlerman, G. Gottstein: Acta Mater. 47 (1999) 3901.
[29] D.A. Molodov, J. Swiderski, G. Gottstein, W. Lojkowski, L.S. Shvindlerman: Acta Metall Mater. 42 (1994) 3397.
[30] D.A. Molodov, G. Gottstein, F. Heringhaus, L.S. Shvindlerman: Acta Mater. 46 (1998) 5627–5632.
[31] P. Lejcek, V. Paidar, J. Adámek, S. Kadecková: Interface Science 1 (1993) 187.
[32] P. Lejcek, J. Adámek: J. Physique IV, 5 (1995) C3–107.
[33] M. Furtkamp, G. Gottstein, D.A. Molodov, V.N. Semenov, L.S. Shvindlerman: Acta Mater. 46 (1998) 4103.
[34] S. Tsurekawa, T. Ueda, K. Ichikawa, H. Nakashima, Y. Yoshitomi, H. Yoshinaga: Mater. Sci. For. 204–206 (1996) 221.
[35] D. Srolovitz: private communication with authors, Institut für Metallkunde und Metallphysik, RWTH Aachen University, March (1998).
[36] T. Surholt, D.A. Molodov, C. Herzig: Acta mater. 46 (1998) 5345.
[37] G. Gottstein, L.S. Shvindlerman: Interface Sci. 6 (1998) 267.
[38] G. Gottstein, L.S. Shvindlerman: Grain Boundary Migration in Metals, Thermodynamics, Kinetics, Applications. Baca Raton, Fl: CRC Press (1999).
[39] K.T. Aust, J.W. Rutter: Trans. AIME 215 (1959) 119.
[40] K.T. Aust, J.W. Rutter: Trans. AIME 215 (1959) 820.
[41] E.M. Fridman, C.V. Kopetskii, L.S. Shvindlerman: Z. Metallkd. 66 (1975) 533.
[42] S. Hoffmann, P. Lejcek: Interface Science 3 (1996) 241.
[43] G. Gottstein, H.C. Murmann, G. Renner, C. Simpson, K. Lücke, in: G. Gottstein, K. Lücke (Eds.), Textures of Materials, Springer Verlag, Berlin (1978) 521.
[44] D.A. Molodov: Dissertation, Moscow (1985).
[45] J.C. Verhasselt, G. Gottstein, D.A. Molodov, L.S. Shvindlerman: Acta Mater. 47 (1999) 887.
[46] D.M. Kirch, B. Zhao, D.A. Molodov, G. Gottstein: Scripta Mater. 56 (2007) 939.
[47] D.M. Kirch, E. Jannot, L.A. Barrales-Mora, D.A. Molodov, G. Gottstein: Acta Mater. 56 (2008) 4998.
[48] V.G. Sursaeva, B.B. Straumal, A.S. Gornakova, L.S. Shvindlerman, G. Gottstein: Acta Mater. 56 (2008) 2728.
[49] E. Rabkin: J. Mater. Sci. 40 (2005) 875.
[50] M. Winning, G. Gottstein, L.S. Shvindlerman: Acta Mater. 50 (2002) 353.
[51] D.M. Kirch: Doctoral Thesis, RWTH Aachen University (2008).
[52] A. Kazaryan, Y. Wang, S.A. Dregia, B.R. Patton: Acta mater. 50 (2002) 2491.
[53] G.S. Rohrer: Annu. Rev. Mater. Res. 35 (2005) 99.
[54] A.P. Sutton, R.W. Balluffi: Interfaces in Crystalline Materials, Clarendon Press, Oxford (1995).
[55] G. Gottstein, H.C. Murmann, G. Renner, C. Simpson, K. Lücke, in: G. Gottstein, K. Lücke (Eds.), Textures of Materials, Berlin, Springer-Verlag (1978) 521.
[56] T.E. Hsieh, R.W. Balluffi: Acta Metall. 37 (1989) 2133.
[57] G.M. Watson, D. Gibbs, S. Song, A.R. Sandy, S.G.J. Mochril, D.M. Zener: Phys. Rev. 52 (1995) 12329.
[58] S.B. Lee, D.Y. Yoon, M.B. Henry: Acta Mater. 48 (2000) 3071.
[59] J.B. Koo, D.Y. Yoon: Metall. Mater. Trans. A 32 (2001) 469.
[60] B.B. Straumal E. Rabkin, V.G. Sursaeva, A.S. Gornakova: Z. Metallkd. 96 (2005) 2.
[61] G. Gottstein, L.S. Shvindlerman, V.G. Sursaeva: Int. Journal of Materials Research 5 (2008) 491–495.
[62] D.A. Molodov, G. Gottstein, F. Heringhaus, L.S. Shvindlerman: Scripta Mater. 37 (1997) 1207–1213.
[63] A. Goetz, A. Focke: Phys. Rev. 45 (1934) 170–199.
[64] G. Gottstein, D.A. Molodov, E. Rabkin, L.S. Shvindlerman, I. Snapiro: Interface Science 10 (2002) 279.
[65] F. Hünning, D.A. Molodov: unpublished work.
[66] P.J. Konijnenberg, D.A. Molodov, G. Gottstein: Mat. Sci. Forum 467 (2004) 763–770.
[67] A.D. Sheikh-Ali, D.A. Molodov, H. Garmestani: Scripta Mater. 48 (2003) 483–488.
[68] V.G. Sursaeva, A.V. Andreeva, C.V. Kopetskii, L.S. Shvindlerman: Phys. Met. Metall. 41 (1976) 4103–4108.
[69] A.V. Antonov, L.S. Shvindlerman: Sov. Phys. Solid State 15 (1973) 1083–1086.
[70] P.J. Konijnenberg, A. Ziemons, D.A. Molodov, G. Gottstein: Rev. Sci. Instrum. 79, 013701 (2008).
[71] H. Fukutomi, R. Horiuchi: Trans. Jap. Inst. Metals. 22 (1981) 633.
[72] H. Fukutomi, T. Kamijo: Scripta Metall. 19 (1985) 195.
[73] H. Fukutomi, T. Iseki, T. Endo, T. Kamijo: Acta Metall. Mater. 39 (1991) 1445.
[74] H. Yoshida, K. Yokoyama, N. Shibata, Y. Ikuhara, T. Sakuma: Acta Mater. 52 (2004) 2349.
[75] A. Suzuki, Y. Mishin: Mater Sci Forum 502 (2005) 157.
[76] D.A. Molodov, V.A. Ivanov, G. Gottstein: Acta Mater. 55 (2007) 1843–1848.
[77] D.A. Molodov, T. Gorkaya, G. Gottstein: Mater. Sci. Forum 558 (2007) 927–932.
[78] T. Gorkaya, D.A. Molodov, G. Gottstein, in: J. Hirsch, B. Skrotzki, G. Gottstein (Eds.), Aluminium Alloys Their Physical and Mechanical Properties, Wiley-VCH (DGM), Vol. 1 (2008) 1071.
[79] T. Gorkaya, D.A. Molodov, G. Gottstein: will be published.
[80] J.W. Cahn, J.E. Taylor: Acta Mater. 52 (2004) 4887–4898.
[81] J.W. Cahn, Y. Mishin, A. Suzuki: Philos. Mag. 86 (2006) 3965–3980.

[82] J.W. Cahn, Y. Mishin, A. Suzuki: Acta Mater. 54 (2006) 4953–4975.
[83] C.J. Smithells, in: Smithells Metals Reference Book, Butterworth, London (1983).
[84] Y. Estrin, G. Gottstein, E. Rabkin. L.S. Shvindlerman: Scripta Mater. 43 (2000) 141.
[85] Y. Estrin, G. Gottstein, L.S. Shvindlerman: Acta Mater. 47 (1999) 3541.
[86] G.S. Knizhnik: Poverhnost: Fizika, Khimia, Mehanika 5 (1981) 50.
[87] D. Wolf: Scripta Metall. 23 (1989) 1913.
[88] D. Wolf: Acta Metall. 38 (1990) 781.
[89] H.J. Frost, M.F. Ashby, F. Spaepen: Scripta Metall. 14 (1980) 1051.
[90] M.A. Stremel, A.L. Markovich: Poverhnost 1 (1997) 85.
[91] H. Meiser, H. Gleiter: Scripta Metall. 14 (1980) 95.
[92] K.L. Merkle, R. Csencsists, K.L. Rynes, J.P. Withrow, P.A. Stadelmann: Journal of Microscopy 190 (1998) 204.
[93] V.A. Ivanov: Doctoral Thesis, RWTH Aachen University, 2006.
[94] V. Fradkov, L.S. Shvindlerman: Fiz. Metall Metalloved 48 (1979) 297.
[95] L.S. Shvindlerman, G. Gottstein, V.A. Ivanov, D.A. Molodov, D. Kolesnikov, W. Lojkowski: Journal of Materials Science 41 (2006) 7725–7729.
[96] V. Ivanov, T. Gorkaya, D.A. Molodov, G. Gottstein, L.S. Shvindlerman, D. Kolesnikov, W. Lojkowski: Acta Mater., in press.
[97] J. Von Neumann: Metal Interfaces, American Society for Testing Materials, Cleveland (1952) 108.
[98] W.W. Mullins: J. Appl. Phys. 27 (1956) 900.
[99] D.M. Kirch: Doctoral Thesis, RWTH Aachen University, 2008
[100] U. Czubayko, V.G. Sursaeva, G. Gottstein, L.S. Shvindlerman: Acta mater. 46 (1998) 5863.
[101] G. Gottstein, L.S. Shvindlerman: Z. Metallkd. 95 (2004) 219–222.
[102] D. Mattissen, A. Wærø, D.A. Molodov, L.S. Shvindlerman, G. Gottstein: Journal of Microscopy 213 (2004) 257–261.
[103] S.G. Protasova, G. Gottstein, D.A. Molodov, V.G. Sursaeva, L.S. Shvindlerman: Acta Mater. 49 (2001) 2519.
[104] V.G. Sursaeva, G. Gottstein, L.S. Shvindlerman, in: G. Gottstein, D.A. Molodov (Eds.), Recrystallization and Grain Growth, Springer-Verlag, Vol. I (2001) 455.
[105] M. Upmanyu, D.J. Srolovitz, L.S. Shvindlerman, G. Gottstein: Acta Mater. 50 (2002) 1405.
[106] M. Upmanyu, D.J. Srolovitz, L.S. Shvindlerman, G. Gottstein: Interface Sci. 7 (1999) 2307.
[107] M. Upmanyu., D.J. Srolovitz, L.S. Shvindlerman, G. Gottstein: Acta Mater. 47 (1999) 3901.
[108] G. Gottstein, L.S. Shvindlerman: Scripta Mater. 52 (2005) 863.
[109] L.A. Barrales Mora, L.S. Shvindlerman, V. Mohles, G. Gottstein: Mat. Sci. Forum, 558 (2007) 1051–1056; Acta Mater. 56 (2008) 1151.
[110] D. Mattissen, D.A. Molodov, L.S. Shvindlerman, G. Gottstein: Acta Mater. 53 (2005) 2049.
[111] G. Gottstein, Y. Ma, L.S. Shvindlerma: Acta Mater. 53 (2005) 1535.
[112] V.E. Fradkov, A.S. Kravchenko, L.S. Shvindlerman: Scripta Metall. 19 (1985) 1291.
[113] V.G. Sursaeva, S.G. Protasova, in: G. Gottstein, D.A. Molodov (Eds.), Recrystallization and Grain Growth, Springer-Verlag, Vol. I (2001) 327.
[114] C.E. Krill, R. Birringer, in: G. Gottstein, D.A. Molodov (Eds.), Recrystallization and Grain Growth, Springer-Verlag, Vol. I (2001) 205.
[115] J.W. Cahn: Trans. Met. Soc. AIME 239 (1967) 610.
[116] W.W. Mullins: Acta metal. 37 (1989) 2979.
[117] S. Hilgenfeldt, A.M. Krynik, S.S. Koehler, H.A. Stone: Phys. Rev. Lett. 86 (2001) 2685.
[118] M.E. Glicksman: Phil. Mag. 85 (2005) 3.
[119] P.R. Rios, M.E. Glicksman: Acta Mater. 54 (2006) 5313.
[120] P.R. Rios, M.E. Glicksman: Acta Mater. 55 (2007) 1565.
[121] R.D. MacPherson, D.J. Srolovitz: Nature 446 (2007) 1053.
[122] P.R. Rios, M.E. Glicksman: Acta Mater. 56 (2008) 1165.
[123] L.A. Barrales Mora, G. Gottstein, L.S. Shvindlerman: Acta Mater. 56 (2008) 5915.
[124] Y. Bréchet, M. Militzer: Scripta Mater. 52 (2005) 1299.
[125] G. Gottstein, L.S. Shvindlerman: Scripta Mater. 54 (2006) 1065–1070.
[126] L. Claudio, D. Castro, B.S. Mitchell: Mat. Sci. Eng. A 396 (2005) 124.
[127] V. Yu. Novikov: Materials Letters 62 (2008) 2071.
[128] M. Ames, J. Markmann, R. Karos, A. Michels, A. Tschöpe, R. Birringer: Acta Mater. 56, (2008) 4255–4266.
[129] I. Majid, P.D. Bristowe: Scripta Metall. 21 (1987) 1153.
[130] P.R.J. Jhan, D. Bristowe: Scripta Metall. Mater. 24 (1990) 1313–1318.
[131] E. Babcock, R. W. Balluffi: Acta Metall. 37 (1989) 367–2376
[132] M. Upmanyu, D.J. Srolovitz, L.S. Shvindlerman, G. Gottstein: Interface Science 6 (1998) 287–298.
[133] B. Schönfelder, D. Wolf, S.R. Phillpot, M. Furtkamp: Interface Science 5 (1997) 245–262.
[134] B. Schönfelder, G. Gottstein, L.S. Shvindlerman: Acta Mater. 53 (2005) 1597–1609.
[135] B. Schönfelder, G. Gottstein, L.S. Shvindlerman: Met. Mat. Trans. A 37 (2006) 1757–1771.
[136] I. Kaur, W. Gust: Fundamentals of Grain and Interphase Boundary Diffusion, Ziegler Press, Stuttgart (1988).
[137] P. Zieba, W. Gust: Interface Sci: 10 (2002) 27–30.
[138] Y. Estrin, G. Gottstein, L.S. Shvindlerman: Scripta Mater. 41 (1999) 385.
[139] Y. Estrin, G. Gottstein, L.S. Shvindlerman: Scripta Mater. 41 (1999) 415.
[140] Y. Estrin, G. Gottstein, E. Rabkin, L.S. Shvindlerman: Acta Mater. 49 (2001) 673.

(Received October 30, 2008; accepted February 13, 2009)

Bibliography

DOI 10.3139/146.110077
Int. J. Mat. Res. (formerly Z. Metallkd.)
100 (2009) 4; page 461–482

ISSN 1862-5282

Correspondence address

Professor Dr. rer. nat. Dmitri A. Molodov
Institut für Metallkunde und Metallphysik
RWTH Aachen University, D-52056 Aachen, Germany
Tel.: +49 241 80 2 6873
Fax: +49 80 22301
E-mail: molodov@imm.rwth-aachen.de

You will find the article and additional material by entering the document number **MK110077** on our website at *www.ijmr.de*